A Novel Pathway of Atmospheric Sulfate Formation Through Carbonate Radical

Yangyang Liu[1,2], Yue Deng[1,2], Jiarong Liu[3], Xiaozhong Fang[1], Tao Wang[1], Kejian Li[1], Kedong Gong[1], Aziz U. Bacha[1], Iqra Nabi[1], Qiuyue Ge[1], Xiuhui Zhang[3], Christian George[4], and Liwu Zhang[1,2]

[1]Shanghai Key Laboratory of Atmospheric Particle Pollution and Prevention, Department of Environmental Science and Engineering, Fudan University, Shanghai, 200433, P. R. China.
[2]Shanghai Institute of Pollution Control and Ecological Security, Shanghai, 200092, Peoples' Republic of China.
[3]Key Laboratory of Cluster Science, Ministry of Education of China, School of Chemistry and Chemical Engineering, Beijing Institute of Technology, Beijing 100081, P. R. China
[4]Univ. Lyon, Université Claude Bernard Lyon 1, CNRS, IRCELYON, F-69626, Villeurbanne, France.

Correspondence to: Liwu Zhang (zhanglw@fudan.edu.cn)

Abstract. Carbon dioxide is considered an inert gas that rarely participates in atmospheric chemical reactions. Nonetheless, we show here that CO_2 is involved in some important photo-oxidation reactions in the atmosphere through the formation of carbonate radicals ($CO_3^{\cdot-}$). This potentially active intermediate $CO_3^{\cdot-}$ is routinely overlooked in atmospheric chemistry concerning its effect on sulfate formation. Present work demonstrates that SO_2 uptake coefficient is enhanced by 17 times on mineral dust particles driven by $CO_3^{\cdot-}$. Importantly, upon irradiation mineral dust particles are speculated to produce gas-phase carbonate radical ions when the atmospherically relevant concentration of CO_2 presents, thereby potentially promoting external sulfate aerosol formation and oxidative potential in the atmosphere. Employing a suite of laboratory investigations of sulfate formation in the presence of carbonate radical on the model and authentic dust particles, ground-based field measurements of sulfate and (bi)carbonate ions within ambient PM, together with density functional theory (DFT) calculations for single electron transfer processes in terms of $CO_3^{\cdot-}$-initiated S(IV) oxidation, a novel role of carbonate radical in atmospheric chemistry is elucidated.

1. Introduction

Atmospheric composition changes are subjected to highly reactive light-induced radicals, such as hydroxyl (·OH), hydroperoxyl ($HO_2\cdot$), or nitrate radicals ($NO_3\cdot$), which are able to alter not only compositions but also physical and chemical properties of particulate matter (Liu et al., 2022a; Mahajan et al., 2021; Stevenson et al., 2020). However, when atmospheric chemical reactions occur over humified particles at ambient conditions, which creates a locally enriched aqueous medium of unique chemical activity, other radicals might likewise gain importance. The carbonate radical ($CO_3^{\cdot-}$) is typically such an active radical. The lifetime of $CO_3^{\cdot-}$ ranges from a microsecond to even a few milliseconds and its concentration can be two

orders of magnitude higher than that of hydroxyl radicals over the water surface (Chandrasekaran and Thomas, 1983; Goldstein et al., 2001; Shafirovich et al., 2001; Sulzberger et al., 1997). In addition, the one-electron reduction potential of $E^0(CO_3^{\cdot-}/CO_3^{2-})$ couple is 1.78 V vs. NHE at neutral pH, leaving $CO_3^{\cdot-}$ a strong oxidant in aquatic chemistry (Bisby et al., 1998; Cope et al., 1973 ; Merouani et al., 2010). Previous studies concerning carbonate radical in aqueous media demonstrate that it reacts rapidly with some organic compounds (Merouani et al., 2010), especially for those electron-rich compounds amines (Stenman et al., 2003; Yan et al., 2019). Also, it has been pointed out that the scavenging of hydroxyl radicals by (bi)carbonate species leads to the formation of $CO_3^{\cdot-}$ ions (Graedel and Weschler, 1981; Xiong et al., 2016). Besides, a high second order of rate constant, lying at 10^9 M^{-1} s^{-1}, has been reported for the reaction of $CO_3^{\cdot-}$ with porphyrins (Ferrer-Sueta et al., 2003), indicating that this radical ion has great oxidation capability that may trigger atmospherically relevant chemical reactions, i.e. secondary inorganic species formation. However, it is only regarded as a marginal intermediate in tropospheric anion chemistry so far (Beig and Brasseur, 2000; Ge et al., 2021; Herrmann et al., 2000; Lehtipalo et al., 2016) and its underlying role as an active oxidant for heterogeneous reaction in the atmosphere is barely explored. Very recently, our group observed the promotional effect of $CO_3^{\cdot-}$ on atmospheric nitrate formation (Fang et al., 2021). Motivated by this finding, attempts were made to further explore its role in other important atmospherically-relevant reactions.

It is well documented that sulfate (SO_4^{2-}) is also a key constituent of aerosols in the atmosphere (Huang et al., 2015; Su et al., 2016). It is able to serve as the precursors of efficient cloud condensation nuclei, with optical properties leading to a cooling effect (Wang et al., 2011). As a consequence, the mechanism aspect of secondary sulfate formation was the focus of numerous studies over the past decades (Hung et al., 2018; Stone, 2002; Zhang et al., 2015b). There is a consensus that high-valence sulfur (VI), produced from the oxidation of anthropogenic SO_2, is the dominant source of atmospheric secondary sulfate. However, a remarkable missing sulfate budget emerges for the atmospheric modeling (Huang et al., 2019; Itahashi et al., 2018; Liu et al., 2021), which significantly underpredicts SO_4^{2-} with respect to observational results when heterogeneous aerosol chemistry is not considered (Feng et al., 2018; Wu et al., 2021; Zheng et al., 2015). This indicates that the heterogeneous sulfate production pathway is a crucial process and exploring the unrecognized heterogeneous mechanism is very likely to narrow the gap between observations in lab studies, field measurements, and numerical modelings. Due to the missing chemical mechanism that initiated fast SO_2 oxidation, atmospheric models fail to capture the key feature of atmospheric observations of high sulfate production during dust storm episodes in the troposphere (Dong et al., 2016; Huang et al., 2014; Yu et al., 2020), where an evident increase of Ca^{2+} (Li et al., 2013; Wang et al., 2005), carbonate-containing particles with high alkalinity (Abou-Ghanem et al., 2020; Li et al., 2014; Tang et al., 2016) as well as photoactive mineral components (Nie et al., 2012; Ta et al., 2003) are prevalent. Air mass is usually in low relative humidity, reported being 25-35 % (Al-Salihi and Mohammed, 2015) (Csavina et al., 2014; Najafpour et al., 2020) in these events, during which the photochemical process is able to alter atmospheric constituents (Liu et al., 2022b). Consequently, there are unknown heterogeneous reaction pathways and previously unconsidered promoters that have great potential to accelerate sulfate formation in the dust storm relevant conditions.

Due to the high stability of CO_2 under ambient conditions (Hossain et al., 2020), there are rare studies concerning the influence of CO_2 in atmospheric chemical processes (Deng et al., 2020; Liu et al., 2020c; Xia et al., 2021). CO_2 is demonstrated

to form (bi)carbonate species over humidified dust particles (Baltrusaitis et al., 2011; Nanayakkara et al., 2014) and reduced to CO under solar illumination (Deng et al., 2020). Nonetheless, its impact on atmospheric heterogeneous reactions remains poorly characterized. Our early laboratory study illustrates that CO_2 decreases the sulfate formation on aluminum oxide particles in the dark (Liu et al., 2020c) while upon solar illumination its role in SO_2 oxidation over mineral dust surfaces is still an open question. In addition, carbonate salt is abundant in authentic dust particles (Cao et al., 2005) and is reported to reach over 10 % wt. of Asian dust particles (McNaughton et al., 2009). It is generally accepted that CO_3^{2-} affects atmospheric chemistry and aerosol characteristics mainly through its intrinsic alkalinity, which buffers aerosol acidity and increases SO_2 adsorption and corresponding sulfate production in the presence of oxidants (Al-Hosney and Grassian, 2005; Bao et al., 2010; Kerminen et al., 2001; Li et al., 2007; Yu et al., 2018). In fact, either CO_2 or carbonate salt is able to produce the active $CO_3^{\cdot-}$ under the ambient circumstance (Ervens et al., 2003; Graedel and Weschler, 1981) and prone to increase the oxidative capacity in the atmosphere. Our early study shows that carbonate radicals serve as an active oxidant to accelerate NO_2 oxidation over mineral dust particles (Fang et al., 2021), allowing us to consider the possibility that fast heterogeneous SO_2 oxidation can be triggered by this active intermediate as well. Nevertheless, to the best of our knowledge, no work has ever considered how and to what extent the carbonate radical influences SO_2 heterogeneous oxidation in the atmosphere.

In the current study, through laboratory studies, we present that carbon dioxide and calcium carbonate, working as the precursor of carbonate radicals, have the ability to accelerate sulfate formation over authentic particles in the atmosphere. Together with quantum chemistry calculations, a detailed molecular mechanism regarding a single electron transfer (SET) process between carbonate radical and sulfite ions is elucidated. Furthermore, ground-based observations validate some findings from the laboratory-based simulations.

2. Experimental methods

2.1 Laboratory Studies

Methodology for uptake coefficient estimation. The reaction uptake coefficient was estimated by the following Eqs. **1**-**3**, as suggested by the previous work (Kong et al., 2014):

$$\gamma=\frac{d[SO_4^{2-}]/dt}{Z} \quad [\mathbf{1}]$$

$$Z=\frac{1}{4}\times A_s\times[SO_2]\times v \quad [\mathbf{2}]$$

$$v=\sqrt{8RT/\pi M_{SO2}} \quad [\mathbf{3}]$$

where v is the mean molecular velocity of SO_2, A_s the effective sample surface, R the gas constant, T the temperature, M_{SO2} the molecular weight of SO_2, and a total number of surface collisions per unit time (*Z*). To be precise, the formation rates

($d[SO_4^{2-}]/dt$) in the equation were determined by ion chromatography (IC) measurements, followed by a conversion factor calculation through linear regression analysis for the integrated absorbance of sulfate bands and corresponding sulfate concentrations. By employing this method, a conversion factor of $f = 6.34\times10^{15}$ ions integrated absorption units^{-1} was obtained and corresponding SO_2 uptake coefficients in the "TiO_2+(CO_2)+SO_2" system were thus estimated using seven timepoints during the heterogeneous reaction. For SO_2 uptake in the "TiO_2+($CaCO_3$)+SO_2" system, we estimated SO_2 uptake coefficients using three conversion curves established for various types of dust particles. For this purpose, we mixed the known proportion of K_2SO_4 and dust particles of concern, and thus obtained relationship curves between the integrated absorbance of DRIFTS (i.e. diffuse reflectance Fourier transformed infrared spectroscopy) sulfate bands and corresponding theoretical sulfate content through linear fitting (Fig. S4). Ten timepoints during the heterogeneous reaction were applied for these kinetics calculations.

Preparation for clay and dust membranes and investigation of sulfate formation on those authentic particles during the daytime and nighttime. Each particle suspension ATD (2.5 mg~0.5 mL), IMt-2 (10 mg~ 0.5 mL) and K-GA (10 mg~ 0.5 mL) were first dispersed into water through ultrasonic bath for 5 min. After that, sample suspensions were transformed onto the cleansed round quartz films (d = 2 cm) using a pipette and subsequently sent to the infrared drying oven for 10 min to prepare dust membranes. Once taken out from the oven, samples were quickly sealed into a desiccator and cooled down to room temperature before starting experiments. A membrane sample was then mounted at the center of the reaction chamber (the top half made of quartz and the bottom half made of Teflon). Before each set of experiments, a gas flow (dry air) of 300 mL min^{-1} was introduced to the chamber for 5 min where a prepared membrane sample was installed. Afterward, samples were exposed to 4.91×10^{14} molecule cm^{-3} SO_2 (+2.46×10^{18} CO_2 when necessary) /N_2+O_2 mixture in the absence and presence of irradiation (Light intensity (I) = 30 mW cm^{-2}) for 15 min before the sample were transferred to a beaker (scale = 10 mL) with 2 mL of 2 % vol. isopropanol leaching solution, extracting ions in the ultrasonic tank for 5 min using 0.22 μm PTFE membrane filter, followed by sending the sample into IC. Noting that dust and clay particles possess a considerable amount of sulfate ion background, we thus measured the background ions for each batch of synthesized dust particle membranes following the procedures described above. All data demonstrated in Fig. 6 were obtained after subtraction of background ions.

Determination of gas-phase reactive oxygen species (ROS) production in the flow-cell reactor. To measure the concentration of ROS released from TiO_2 particles in various reaction systems, an experimental approach using the probe molecule aniline was applied in this study. This is because compound aniline is reported to react rapidly with ·OH radicals and $CO_3^{\cdot-}$ radicals, which are also evidenced to be two major active ROS species that are responsible for the SO_2 oxidation over mineral dust particles. The method applied in this study was almost implemented as the same to that of the previous study (Behrman, 2018), with slight modification. Briefly, the degradation rate of aniline in various reaction systems were monitored through High-Performance Liquid Chromatography (HPLC, LC-10AD, SHIMADZU, Japan). A Zorbax SB C18 (4.6 mm × 150 mm, 5 μm) reverse phase column at 25 ℃ was used with a UV detector at 236 nm to measure the aniline concentration. The mobile phase consisted of acetonitrile/water = 55:45 (V/V) with a flow rate of 1 mL/min.

TiO_2 suspension (5 mg TiO_2 per 100 uL deionized water) was deposited onto the glass substrate (0.13 - 0.17 mm in thickness) using a pipette and then dried in an oven for 10 min to obtain a TiO_2-coated film. Dilute aniline solution, using 67 mM phosphate buffer solution (pH = 7.0), was prepared and placed below the TiO_2-coated film, with an intervening gap between TiO_2 film and solution surface around 2 mm (Fig. 1). This short distance essentially guarantees gaseous ROS (e.g. ·OH radicals or $CO_3^{\cdot-}$ radicals) to diffuse and react with aniline molecule (Rodriguez et al., 2013).

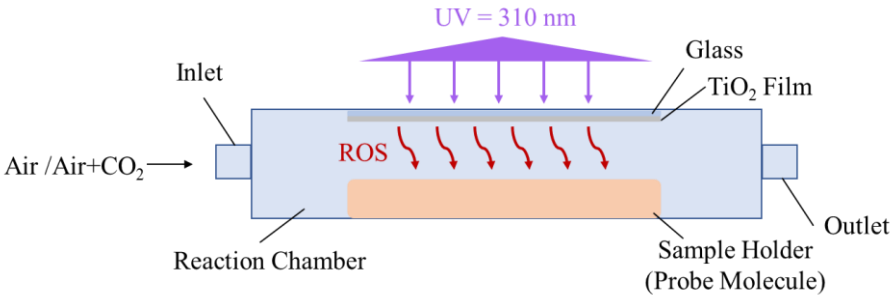

Figure 1. The schematic of the flow-cell reaction chamber for gaseous ROS determination.

In the reaction system containing TiO_2 film upon irradiation (the UV wavelength = 310 nm) in the presence of humidified air (RH = 30 %), when operated in a continuous mode, the overall degradation rate of probe molecules in the presence of TiO_2 film can be described by Eq. **4** (Wang et al., 2004):

$$k_{obs}=\frac{d[An]}{dt}=r_A+r_U+r_{ROS}=r_A+r_U+k_{ROS,\,AN}[ROS][An] \quad [4]$$

Where k_{obs} is the observed degradation rate of aniline, [An] is the concentration of aniline, denoted as [An] hereafter, and r_A, r_U , r_{ROS} stand for aniline removal rates resulting from air stripping, UV photolysis, ROS oxidation. $k_{ROS,\,An}$ are the overall second-order reaction rate constants for An with ROS.

Reference experiments without the introduction of ROS were also conducted to measure r_A+r_U in each reaction system. Upon irradiation, the dust proxy TiO_2 produces hole-electron pairs, further forming ·OH radicals and superoxide radicals ($O_2^{\cdot-}$) in the presence of absorbed water and oxygen molecules. Thus, an experiment using N_2 was adopted to investigate the role of $O_2^{\cdot-}$ in consuming aniline. As illustrated in Fig. 7c, a slight change in the degradation rate of aniline after stripping oxygen from the air, indicating that $O_2^{\cdot-}$ shows quite a smaller contribution than ·OH. This result agrees well with the finding reported by Durán et al. (Duran et al., 2019), where the removal of $O_2^{\cdot-}$ by adding benzoquinone (BQ) into TiO_2 suspension results in the negligible change of An degradation rate.

Taken above, ·OH radicals are assumed to be the only active ROS that accounts for the An degradation. Hence, the maximum steady concentration of ·OH radicals can be given by the following equation:

$$-\frac{d[An]}{dt}=k_{exp}[An]=k_{\cdot OH,\,An}[\cdot OH]_{ss\text{-}max}[An] \quad [5]$$

Integration of Eq. **5** yields

$$-\ln\frac{[An]_t}{[An]_0}=k_{exp}t \quad [6]$$

$$k_{exp}=k_{\cdot OH,An}[\cdot OH]_{ss\text{-}max} \quad [7]$$

Together with the reported second-order rate constant ($k_{\cdot OH,\,An}$ = 6.5×10^9 $M^{-1}s^{-1}$) (Samuni et al., 2002), the steady-state OH radical concentration $[\cdot OH]_{ss\text{-}max}$ in buffered An solution can be calculated from Eq. **7**. The observed degradation rate constant of k_{exp} can be obtained from the slope of the semi-log plot of An degradation as illustrated in Eq. **6**. The maximum steady-state aqueous concentration of ·OH supplied by the partitioning process from gas-phase ·OH was thus estimated to be 2.15 $\times10^{-15}$ M for the "TiO_2+Air" system.

When CO_2 (400 ppm, atmospheric relevant concentration) is introduced into a flow-cell chamber, an increased degradation rate of An is seen, which is very likely to be the generation of active carbonate radical ions (Fig. 9). Similar to the method we adopted for the estimation of $[\cdot OH]_{ss\text{-}max}$, reference experiments were conducted to determine the rates for air stripping and UV photolysis processes in the "TiO_2+Air+CO_2" system. In the next step, we quenched the hydroxyl radicals by adding tertiary butanol (TBA). This is because it reacts rapidly with hydroxyl radicals (Li et al., 2020) $k_{\cdot OH,TBA}$= (6×10^8 M^{-1} s^{-1}) while shows a rather low reaction rate with carbonate radicals (Liu et al., 2015) ($k_{CO_3^{\cdot-},TBA}$<1.6×10^2 M^{-1} s^{-1}). Subsequently, we determined $[CO_3^{\cdot-}]_{ss}$ using the previous protocol (Huang and Mabury, 2000) with known $k_{CO_3^{\cdot-},AN}$ (5.4×10^8 M^{-1} s^{-1}) (Wojnarovits et al., 2020). In the extreme case, assuming that all hydroxyl radical ions were fully trapped by absorbed and dissolved HCO_3^-/CO_3^{2-}, the maximum steady-state $CO_3^{\cdot-}$ concentration was determined to be 1.39×10^{-13} M for "TiO_2+Air+CO_2" system, matching well with the early study where the concentration of $CO_3^{\cdot-}$ is reported to be two orders of magnitudes than ·OH over the water surface (Sulzberger et al., 1997).

2.2 Quantum Chemical Calculation

We employed density functional theory (DFT) calculations in the term of the single electron transfer (SET) process using Gaussian 09 package to investigate this novel route, detailed in Supplementary text 11 and 20.

2.3 Field Observations

Sampling. Our sampling for atmospheric particle matter was launched on the roof of the environmental science and engineering department, Fudan University (Jiangwan Campus, 31.340661°N, 121.506747°E, 16 km away from the city downtown. More geographical information for sampling has been described in detail elsewhere (Liu et al., 2020c). Observations for water-soluble ionic components of particulate matter were performed using an 8-stage non-viable-cascade-impactor type sampler (TISCH TE Inc., USA), size gradient of which are in the sequence of < 0.43, 0.43- 0.65, 0.65-1.1, 1.1-2.1, 2.1- 3.3, 3.3- 4.7, 4.7- 5.8 5.8- 9.0 and 9.0~ μm. These sizes represent the effective cutoff diameter at each level for unit density spherical particles. In our sampling, the estimations for (bi)carbonate ions in atmospheric particulate matter is conducted for the initial four stages (3.3~ μm). Atmospheric airflow from the head was maintained at the constant rate of 28.3

L min^{-1} to meet the operation criterion required for the Anderson-type sampler. Quartz filters (81 mm in diameter, Whatman, GE Healthcare, UK) were applied for samplings, and membranes were rinsed with ultrapure water (electrical resistivity= 18.2 MΩ) no less than three times; that is kept in the ultrasonic cleaning tank for 40 min and then rinsed with ultrapure water for twice, before being sent into the infrared drying oven, followed by packing them in aluminum foils prior to field sampling. We carried out this procedure to eliminate the water-soluble background ions as much as possible and to ensure the balance calculation for (bi)carbonate ions. Additionally, following the same aforementioned pretreatments, we measured the background concentrations of ions in blank membranes. We separated our daily samplings into two periods, 11 hours for each, to give an insight into the influence of potential photo-induced reactions on secondary sulfate formation in the atmosphere.

(Bi)carbonate estimation. The concentration of bi(carbonate) ions were estimated following the protocol reported in the early works (Fang et al., 2021; Liu et al., 2020c; Palmer and Cherry, 1984; Zhang et al., 2011). Two assumptions were made to simplify the estimation for bi(carbonate) concentrations within the system: a. dominating cations in each system are H^+, Li^+, Na^+, NH_4^+, K^+, $Mg^{2+}$and Ca^{2+} whereas those transition and heavy metal ions were out of consideration considering their limited contents of dissolve cations in the atmospheric particulate matter; b. three typical organic acid ions (CH_3COO^-, $COOH^-$ and $C_2O_4^{2-}$, major soluble organic acid ions in the atmosphere) were taken into account for ionization balance and the rest of the charge gap in each system was assumed to originate from (bi)carbonate ions. Then we established balance equations (Eqs. **8-11**) for each sample on the basis of charge conservation and ionization equilibrium constant of carbonic acid (K_1= 4.47×10^{-7} and K_2= 4.69×10^{-11}at 273 K).

$$[H^+]+[Li^+]+[Na^+]+[NH_4^+]+[K^+]+2[Mg^{2+}]+2[Ca^{2+}]=[OH^-]+[F^-]+[CH_3COO^-]+[COOH^-]+[NO_2^-]+[Cl^-]+[NO_3^-]+$$

$$3[PO_4^{3-}]+2[SO_4^{2-}]+2[C_2O_4^{2-}]+[HCO_3^-]+2[CO_3^{2-}] \quad [8]$$

$$[HCO_3^-]=\frac{K_1[H_2CO_3]}{[H^+]} \quad [9]$$

$$[CO_3^{2-}]=\frac{K_1K_2[H_2CO_3]}{[H^+]^2} \quad [10]$$

It is worth mentioning that [X] is referred to charge concentration for ions (Coulomb·M). Additionally, the temperature factor was also considered to correct the equilibrium constant for (bi)carbonate ions using the following equation:

$$\mathrm{Ln}\frac{K_{x'}}{K_x}=-\frac{\Delta H}{R}\left(\frac{1}{T_{x'}}-\frac{1}{T_x}\right) \quad [11]$$

where ΔH is the temperature variation (K), R the ideal gas constant (8.31451 J·mol^{-1}·K^{-1}), and T the temperature (K) during

pH measurements. We then solved those equations to obtain a series of $[HCO_3^-]$, which were eventually corrected by subtracting blank values.

2.4 Other measurements and analysis

In addition to the above descriptions of measurements and calculation methodologies, more information including heterogenous reaction set-up, kinetics reaction order determination, pretreatment of mineral dust, DRIFTS, IC, Raman measurements, and analysis, etc. are available in the supplementary text 1-13.

3. Results and discussion

3.2.1 Accelerated sulfate production in the presence of carbonate.

The physico-chemical properties of employed mineral dust proxies including BET surface area, crystal phase, and structure were first characterized (Fig. S1), consistent with early studies (Balachandran and Eror, 1982; Shang et al., 2010; Su et al., 2008), with additional discussion in supplementary text 14. The spectral irradiance of the solar simulator applied in the present study is well covered by natural sunlight (Fig. S2), as much as possible having experimental results from the lab simulate the real atmosphere. Upon solar irradiation under RH of 30 % SO_2/N_2+O_2 flow ($[SO_2]$ =2.21×10^{14} molecules cm^{-3}), the sulfate production on TiO_2+$CaCO_3$ mixture particles (50 wt. % TiO_2 and 50 wt. % $CaCO_3$), measured by IC, is significantly enhanced by 7 times and 23 times compared to that of pristine TiO_2 and $CaCO_3$ (Fig. 2a), respectively. In stark contrast, there is a negligible increase in sulfate production detected in the TiO_2+$CaCO_3$ mixture relative to that of pristine $CaCO_3$ and TiO_2 in dark experiments (Fig. S3). Great discrepancies in sulfate production over TiO_2+$CaCO_3$ particles between dark and light experiments suggest that carbonate salt may play a different role in these two scenarios. However, the alkalinity of carbonate salt favors SO_2 adsorption (Al-Hosney and Grassian, 2005; Yu et al., 2018) and the photo-oxidation process assisted by TiO_2 particles is able to strengthen the oxidation efficiency of adsorbed SO_2 (Chen et al., 2012; Shang et al., 2010), which is a plausible explanation for increased sulfate production over TiO_2+$CaCO_3$ particles. Following this speculation, two types of mixtures TiO_2+$CaCO_3$ and TiO_2+CaO were employed. In the dark experiments (Fig. 2b), both TiO_2+CaO and TiO_2+$CaCO_3$ almost yield an identical concentration of sulfite and sulfate. On the contrary, TiO_2+$CaCO_3$ particles produce nearly two times of sulfate than TiO_2+CaO particles once irradiated, along with a sharp decrease of S(IV) species on the surface of TiO_2+$CaCO_3$ surfaces. Besides, $CaCO_3$ tends to show relatively humble physical properties including BET surface area, surface pH, as well as solubility, etc. relative to CaO (see detailed discussion in supplementary text 15). The above results allow us to assert that the carbonate-containing system contains an alternative important mechanism for sulfate formation beyond the production of an alkaline environment (additional discussion available in supplementary text 16). Fig. 2c and 2d illustrate that the DRIFTS features of S(IV) and S(VI) species (Nanayakkara et al., 2014; Wu et al., 2011) increase over time on theoretical and experimental TiO_2+$CaCO_3$ mixtures (wt./wt. = 50/50) upon irradiation. The "theoretical" is calculated based on the DRIFTS

experiments of pristine TiO_2 and $CaCO_3$ particles through a simple linear superposition whereas the "experimental" is directly derived from the DRIFTS experiment of TiO_2+$CaCO_3$ (wt./wt. = 50/50) particles. These results suggest a synergistic effect presented in this mixture for sulfate formation under solar irradiation.

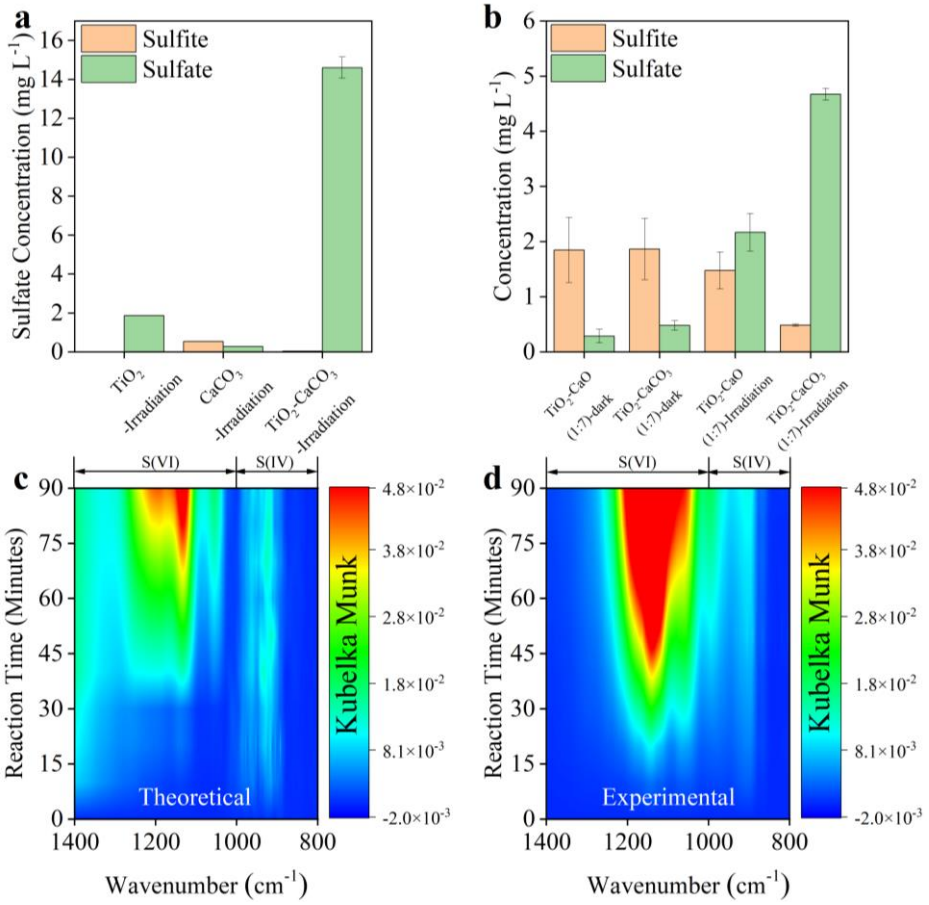

Figure 2. (**a**) Sulfate or sulfite concentration quantified by IC on TiO_2, $CaCO_3$, TiO_2+$CaCO_3$ particles (wt./wt. = 50/50) after exposure to gaseous SO_2 under irradiation for 60 min. **(b)** Sulfate and sulfite concentration quantified by IC on mineral dust particles of concern after exposure to SO_2 under dark or irradiation for 20 min. *In situ* DRIFTS of S(IV) and S(VI) production on theoretical **(c)** and **(d)** experimental TiO_2+$CaCO_3$ mixtures (wt./wt. = 50/50) upon irradiation for 90 min. All spectra were processed by the Kubelka-Munk (K-M) algorithm. Noting that the production of sulfur species in theoretical TiO_2+$CaCO_3$ mixtures refers to 0.5 × K-M bands of sulfur species of TiO_2 + 0.5 × K-M bands of sulfur species of $CaCO_3$ while that for experimental TiO_2+$CaCO_3$ mixtures refers to 1 × K-M bands of sulfur species of TiO_2+$CaCO_3$ mixtures (wt./wt. = 50/50). Reaction conditions: RH = 30 %, Light intensity (I) = 30 mW cm^{-2}, Total flow rate = 52.5 mL min^{-1} and SO_2 = 2.21×10^{14} molecules cm^{-3}.

Combining DRIFTS experiments with the obtained calibration curve (Fig. S4), we estimated that the uptake coefficient of TiO_2+$CaCO_3$ mixture (50 wt. % $CaCO_3$) is increased by about a factor of 17 as compared to that of pure $CaCO_3$ or TiO_2 (Table S1). More importantly, upon irradiation, SO_2 uptake coefficients for these dust mixtures lie at the order of magnitudes of 10^{-4}, which is proven to gain importance in overall sulfate production by numerical modeling investigations (Wang et al., 2014; Zhang and Carmichael, 1999). Hence, the photochemical pathway associated with carbonate species is likely a potential

driving force to increase sulfate production in the atmosphere. Meanwhile, the reaction order of SO_2 in "TiO_2+$CaCO_3$+SO_2" reaction system in the range of 400-20000 ppb is determined to be 0.80 (Fig. S5), indicating that the uptake coefficients obtained at the ppm level of SO_2 would somewhat overestimate the real one obtained at atmosphere relevant SO_2 concentration level (several or a few tens ppb). While we note that the difference between the lab and atmospheric conditions regarding SO_2 concentration remains even after considering the 400 ppb case, employing hundreds of ppb SO_2 in the laboratory simulation to obtain the kinetic parameter of sulfate formation is acceptable (Liu and Abbatt, 2021; Liu et al., 2020b). Therefore, we tentatively believe that uptake coefficients estimated in this work would be valid after being calibrated.

High-resolution transmission electron microscopy (HRTEM) analysis of TiO_2 (50 wt. %) +$CaCO_3$ (50 wt. %) particles after reaction, in combination with energy dispersive spectrometer mapping measurements of sulfur component, was conducted to investigate the synergistic effect between TiO_2 and carbonate ions (Fig. 3 a-d and Fig. S6). A region with a relatively high density of sulfur species was selected for further observation (Fig. 3a and 3b) and the distribution of each component was determined by fast Fourier transformation (FFT) and inverse FFT analyses (panel d) of the selected HRTEM image in high resolution with lattice fringes shown in Fig. 3c. Observation of crystalline $Ti(SO_4)_2$ and $CaSO_4$ on the interface of TiO_2 and $CaCO_3$ components imply that the synergistic effect on sulfate production likely originates from interplays of those two types of components under solar illumination.

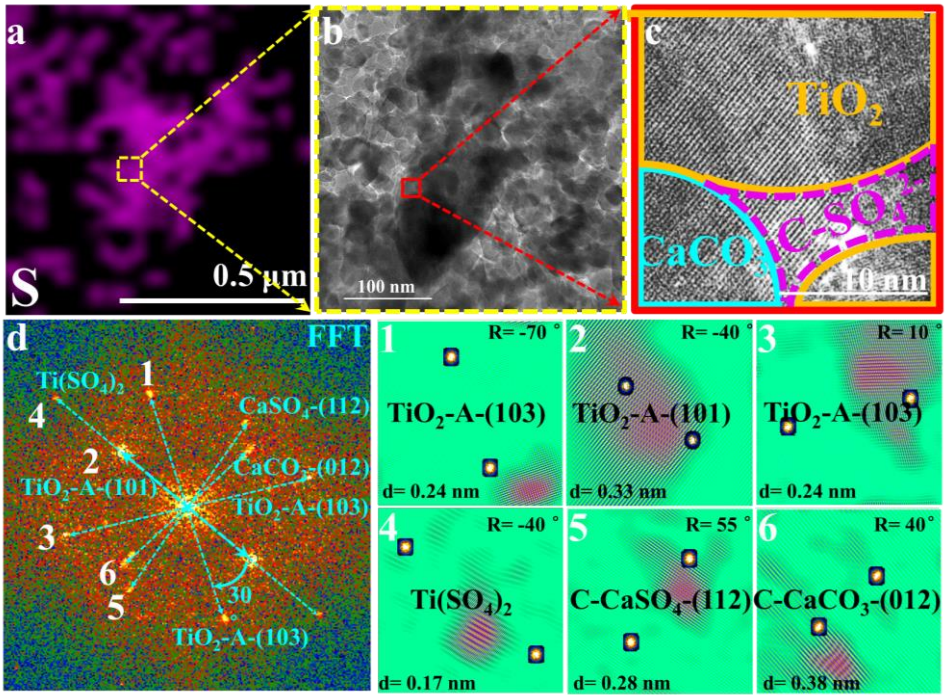

Figure 3. (**a**) Energy Dispersive Spectroscopy (EDS) mapping of sulfur. (**b**) Selected HRTEM region containing a high density of sulfur for further observation and the red rectangle refers to the region shown in panel c. (**c**) The HRTEM image in high resolution with lattice fringes and (**d**) corresponding FFT power spectra, lattice indexing, and (1-6) inverse FFT analysis of lattice signal shown in panel d. In panel c, the term C-SO_4^{2-} stands for crystalline SO_4^{2-}, i.e. $CaSO_4$ and $Ti(SO_4)_2$. Particles employed for the HRTEM measurement refer to TiO_2 (50 wt. %) +$CaCO_3$ (50 wt. %) mixture particles upon exposure to the 4.42×10^{14} molecules cm^{-3} SO_2/N_2+O_2 for 60 min while other reaction conditions

are as same as that of above sulfate quantification experiments in Fig.1. Reaction conditions: RH = 30 %, Light intensity (I) = 30 mW cm^{-2}, Total flow rate = 52.5 mL min^{-1}.

We further assessed the importance of interfacial contact between TiO_2 and $CaCO_3$ in sulfate production by two synthesis approaches in which the interface abundance is modulated for comparison. Typically, a "grinding" method was used to make TiO_2+$CaCO_3$ mixture with compact contact between those two components, thus leading to abundant interfaces. Meanwhile, the "shaking" method is designed to create a TiO_2+$CaCO_3$ mixture of loose contact, leaving relatively fewer amounts of interfaces within the mixtures. The resulting mixing statuses of the two samples meet our expectations, evidenced by the scanning electron microscope (SEM) technique (Fig. S7). IC quantification analysis suggests that particles with considerable junctions exhibit a more pronounced promotion for sulfate production than those having relatively few junctions (Fig. S8). These results emphasize the importance of an indispensable interface contact between TiO_2 and $CaCO_3$ in fast production upon irradiation.

Table1. Chemical compositions of mineral dust simulants.

	SiO_2 (wt. %) †	Al_2O_3 (wt. %) †	$CaCO_3$ (wt. %) *,†	TiO_2 (wt. %) †	‡Ca:Al (Fe:Al)
SiO_2+Al_2O_3	89.46	10.54	-	-	-
SiO_2+Al_2O_3+$CaCO_3$	82.47	9.72	7.81	-	0.73 (-)
SiO_2+Al_2O_3+TiO_2	88.42	10.42	-	1.15	-
SiO_2+Al_2O_3+TiO_2 +$CaCO_3$	81.59	9.62	7.73	1.06	0.73 (-)
ATD	71.27	8.4	-	0.93	0.73 (0.17)

*In the present study, $CaCO_3$ was taken as representative of alkaline-earth metal oxide in our proxies for the authentic dust.

†The mass ratio of 4 components (if any) in the simulants were controlled in the ratio of SiO_2:Al_2O_3:$CaCO_3$: TiO_2= 81.59: 9.62:7.73:1.06. For instance, the mass ratio of SiO_2 to Al_2O_3 is 81.59: 9.62 in the SiO_2+Al_2O_3 simulant whereas is 81.59: 9.62:7.73 in the SiO_2+Al_2O_3+$CaCO_3$ mixture. The ratios of each component are derived from the EDS mapping analysis of ATD dust particles.

‡This column refers to the molar ratio.

The increased sulfate production was further probed by employing mineral dust simulants where two dominant crust constituents SiO_2 and Al_2O_3 were introduced into TiO_2+$CaCO_3$ particles to mimic the authentic mineral dust particles in the atmosphere, with specific component and corresponding ratio information shown in Table 1. It is worth mentioning that the determination of the ratio of each component in the simulants relies upon the EDS mapping results of ATD particles. In Fig. 4, the introduction of TiO_2 components ($\approx$ 1 % wt.) into SiO_2+Al_2O_3 leads to 81.6 % enhancement of sulfate production because of photolabile ROS. On the other hand, merely 24.8 % wt. increase of sulfate yield was observed once $\approx$ 8 % wt. of $CaCO_3$ was incorporated into SiO_2+Al_2O_3 dust particles. This can be attributed to the alkaline environment created by $CaCO_3$,

which is thought to increase SO_2 adsorption (Al-Hosney and Grassian, 2005) and sulfate production accordingly. Surprisingly, mixing of ≈ 1 % mass fraction of TiO_2 and ≈ 8 % wt. of $CaCO_3$ into SiO_2+Al_2O_3 gives rise to a 235 % increase in sulfate formation relative to that of SiO_2+Al_2O_3. It represents nearly an extra 100 % enhancement of sulfate production due to the presence of TiO_2 and $CaCO_3$ of an atmospherically relevant mass fraction. These results lead to the hypothesis that the observed synergistic effect on heterogeneous oxidation of SO_2 is likely to take effect in the atmosphere.

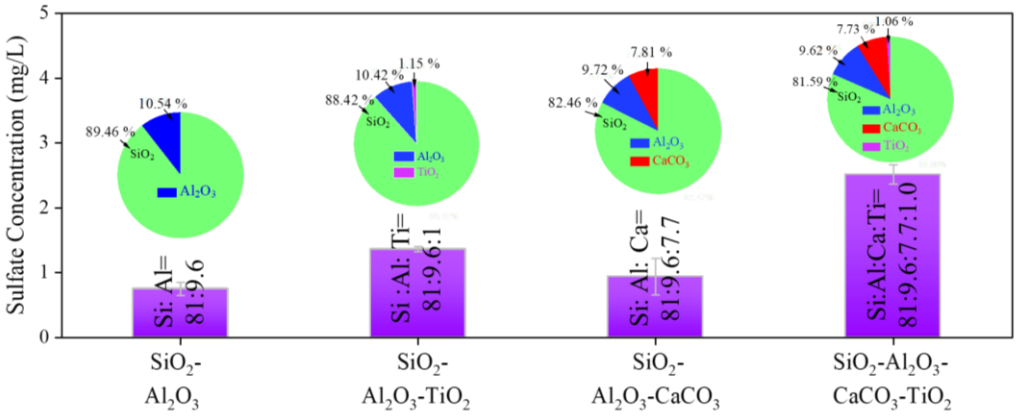

Figure 4. Sulfate concentration quantified by IC. Sulfate concentration was measured by IC on mineral dust simulants after exposure to gaseous SO_2 (2.46×10^{14} molecule cm^{-3}) under irradiation. Noting that SiO_2: Al_2O_3: $CaCO_3$: TiO_2 refers to the mass fraction ratios of the components in simulants. Experiments were all conducted at RH of 30 % and Light intensity (I) of 30 mW cm^{-2}.

Fe_2O_3 is also one of the crucial components found in authentic mineral dust (El Zein et al., 2013), and it has been reported to produce electron-hole pairs under solar irradiation (Li et al., 2019), thus likely involving the reaction channel considered in this work (see detailed discussion in the later section). Similar to the protocol applied for synthesizing the TiO_2+$CaCO_3$ mixture, αFe_2O_3+$CaCO_3$ are accordingly prepared. In Fig. S9a, our results show that αFe_2O_3 can not trigger fast SO_2 oxidation in the presence of carbonate ions upon irradiation, which is distinguished from the results we derived from TiO_2+$CaCO_3$ mixture. This can be explained by the fact that Fe_2O_3 shows a lower redox activity relative to TiO_2 (Fig. S9b), where its strong redox capability essentially enables photo-induced electrons and holes to produce $O_2^{\cdot-}$ and ·OH radical ions. In stark contrast, the valence band and conduct band of Fe_2O_3 lie at -0.18 and at 1.68 V vs. NHE (pH = 7), lower than the redox potential required for generating $O_2^{\cdot-}$, ·OH as well as carbonate-containing ROS (Li et al., 2016). Hence, no promoted sulfate production is seen for αFe_2O_3+$CaCO_3$ particles under irradiation. We also note the inconsistency between our study and the previous literature with regard to the response of SO_2 oxidation to solar irradiation over αFe_2O_3 particles, which has been interpreted in supplementary text 17.

Overall, we show that upon irradiation atmospherically relevant content of TiO_2 (nearly 1 %) in mineral dust simulants is able to interact with carbonate ions to launch an increased sulfate production, which is beyond the conventional regime of

alkaline neutralization of H_2SO_4. Unlike TiO_2, αFe_2O_3 lacks the ability to initiate fast SO_2 oxidation by generating carbonate-containing ROS due to its limited photo-chemical activity although ferric chemistry is important in secondary sulfate formation in the atmosphere (Sullivan et al., 2007; Yermakov and Purmal, 2003).

3.2.2 Accelerated sulfate production in the presence of CO_2.

Atmospheric CO_2 is also an important source of (bi)carbonate. Its influence on photochemical SO_2 uptake on mineral dust was thus studied. Distinguishing S(VI) from S(IV) species over TiO_2 particles relies upon the position of the IR bands according to the assignment of previous literature (Nanayakkara et al., 2014), and S(VI) and S(IV) build up as heterogeneous reactions proceed in all cases (Fig. 5). In the presence of atmospherically relevant CO_2 (9.83×10^{15} molecules cm^{-3}), sulfate yield was increased under irradiation as compared to the CO_2-free case (Fig. 5a and b). We cautiously examined the net effect of formed (bi)carbonate on sulfate production by time-resolved DRIFTS spectra (Fig. 5c and d) using dark experiments. CO_2 suppresses both S(IV) and S(VI) products in the dark probably because of the competitive adsorption effect, as we observed over Al_2O_3 particles (Liu et al., 2020c).

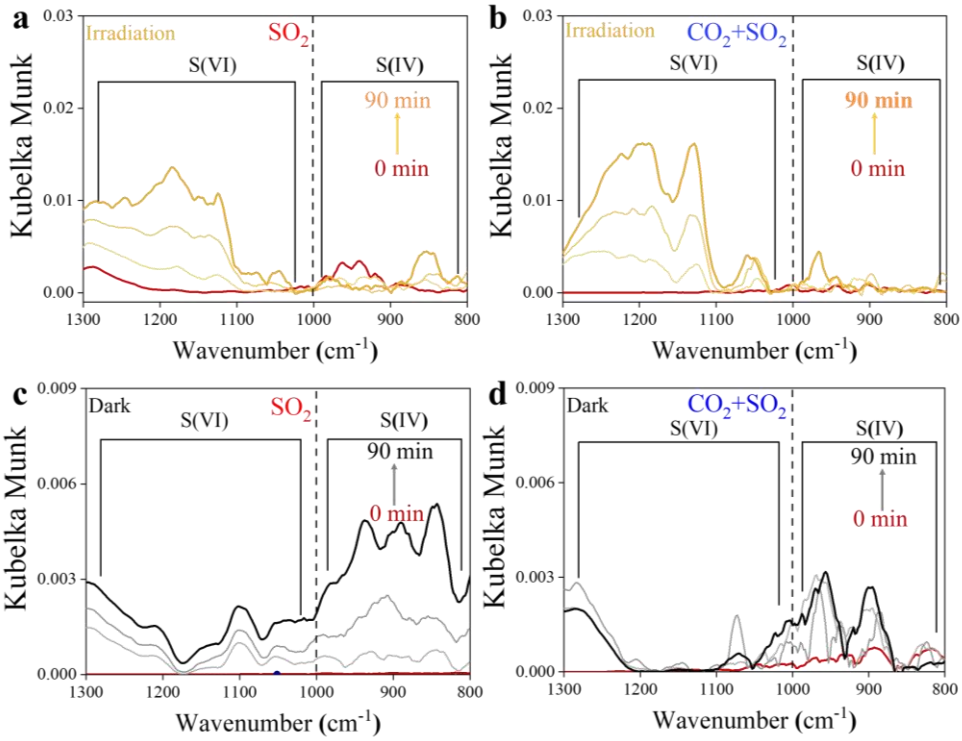

Figure 5. Time-resolved DRIFTS of S(IV) and S(VI) products over TiO_2 particles after exposure to SO_2/N_2+O_2 in the absence and presence of CO_2 upon irradiation (**a** and **b**) and those reactions under dark (**c** and **d**). Reaction conditions: RH = 30 %, Light intensity (I) = 30 mW cm^{-2}, total flow rate = 52.5 mL min^{-1} and $SO_2 = 7.37\times10^{13}$ molecules cm^{-3}.

Above observation leads us to speculate that the active intermediate derived from (bi)carbonate species upon irradiation is a plausible force to drive rapid sulfate formation. Besides, a nearly 50 % increase in SO_2 uptake coefficient is observed for the

mineral dust proxy TiO_2 after being exposed to 9.83×10^{15} molecules cm^{-3} (400 ppm) CO_2+SO_2/N_2+O_2 mixture (Table S1). The pseudo-first reaction order (1.13) was also determined in the selected concentration range of 400-20000 ppb (Fig. S5b), which satisfies the prerequisite for uptake coefficients derived from laboratory chambers potentially being generalized to the atmosphere condition, as we expounded in the early context.

Table 2. Chemical Compositions of the ATD Dust and Standard Clays.

Minerals	ATD (%)*	IMt-2 (%)*	KGa-2 (%)*
SiO_2	78.11	59.57	56.93
Al_2O_3	7.19	19.47	37.49
Fe_2O_3	2.57	7.95	1.81
FeO	n.d. †	0.05	0.15
MgO	1.22	2.42	0.03
CaO	3.03	0.37	0.01
Na_2O	1.39	0.08	n.d. †
K_2O	2.06	8.72	0.06
TiO_2	0.46	0.99	3.43
P_2O_5	0.10	0.07	0.05
MnO	0.04	0.03	n.d.†
S	n.d. †	0.03	0.02
Total	99.21	99.75	99.98
Total A.E. ‡	7.70	11.59	0.10

*Chemical compositions of the dust and clays were determined by XRF results.

†n.d. refers to not detected.

‡A.E. refers to alkaline earth metal oxide.

As another step toward a real scenario in the atmosphere, experimental trials employing authentic mineral dust particles, i.e. K-Ga-2 (Kaolin, Georgia, USA), Arizona test dust (ATD), and clays IMt-2 (Illite, Mont., USA) were implemented, with component analysis results shown in Table 2. In Fig. 6, the pronounced increase in sulfate yield (by nearly 100 % increased sulfate production in the CO_2-involved case under irradiation) is best seen in K-Ga-2 clay (panel a). The promotional effect of CO_2 on sulfate formation under irradiation, nonetheless, is less evident for IMt-2 (the content of $TiO_2 \approx 0.99$ %) and ATD (the content of $TiO_2 \approx 0.46$ %) as compared to K-Ga-2 particles. This may correlate to their higher mass fraction of alkaline earth metal oxide (denoted as A.E.), which enables dust particles to possess a substantial number of (bi)carbonate species within the natural environment where they have experienced long-term exposure to atmospheric CO_2 during the regional transport. Therefore, the aforementioned synergetic effect takes effect over IMt-2 and ATD particles even without exposure

to CO_2 presumably due to the presence of abundant alkaline carbonate formed, and a relatively moderate increase in sulfate production was thus observed. On the other hand, TiO_2 content is not necessarily an accurate predictor of photoreactivity, the content and proportion of the active phase of TiO_2 in K-Ga-2 altogether contribute to a more pronounced increase in sulfate production relative to the other two clays (see detailed discussion in supplementary text 18).

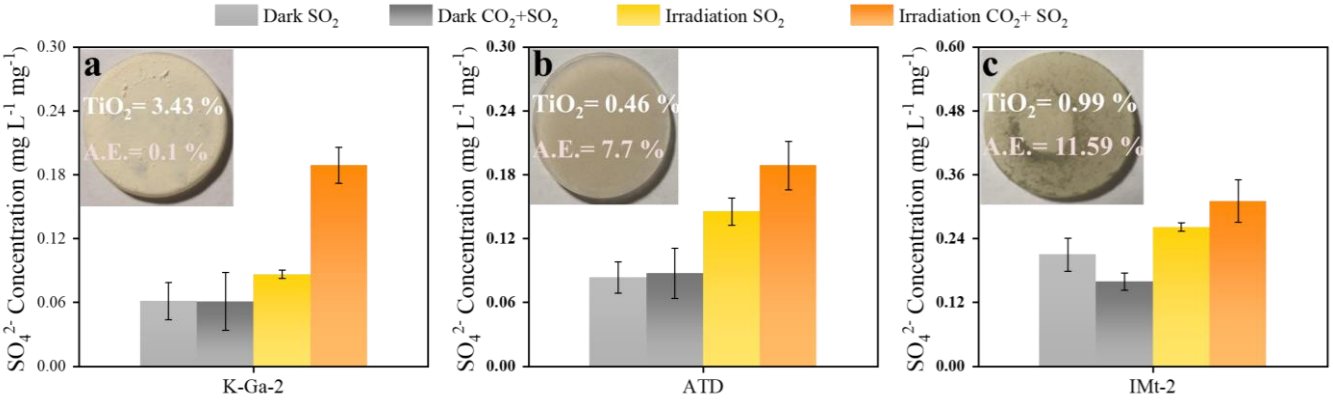

Figure 6. Laboratory studies of sulfate production on authentic dust and clay membranes **(a)** K-Ga-2 **(b)** ATD as well as **(c)** IMt-2 under the dark and irradiation (30 mW cm^{-2}) upon exposure to 4.91×10^{14} molecules cm^{-3} SO_2/N_2+O_2 and 2.46×10^{18} molecules cm^{-3} CO_2+ 4.91×10^{14} molecules cm^{-3} SO_2/N_2+O_2 at RH of 30 %. Noting that sulfate yield in three cases was normalized by the mass of dust particles employed for heterogeneous reaction.

3.2.3 Reaction Mechanism.

The heterogeneous reaction of SO_2 on dust particles in the atmosphere is a complicated process, covering a series of reactions taking place in both homogeneous and heterogeneous ways. At a sufficiently low RH condition (normally below 10 % RH), water readily dissociates on the surface of metal oxide under ambient atmospheric conditions, where the metal oxide surface is terminated by hydroxyl groups that hydrogen bond to adsorbed water molecules (Cwiertny et al., 2008). In this case, SO_2 oxidation over dust particles is dominated by the reaction regime where the resulting hydroxyl groups react with gaseous SO_2 to form adsorbed $S(IV)_{ad}$ species. Afterward, $S(IV)_{ad}$ will be oxidized by oxidants in the atmosphere or photo-induced active intermediates produced from the dust surface upon irradiation. As the RH increases beyond 10 % -15 %, multilayer water coverage occurs, reaching approximately two monolayers at RH of 30 % (Mogili et al., 2006). Under these circumstances, the amount of water adsorbed onto the surface of the dust particles is believed to be sufficiently large that it is liquid-like in corresponding physical and chemical properties (Cwiertny et al., 2008) (Peters and Ewing, 1997). In this work, heterogenous SO_2 oxidation over mineral dust proxies proceeds at the RH of 30 %, and two water layers are likely to attach to dust particles. Thus, radical ions are anticipated to play a key role in fast SO_2 oxidation over humidified mineral dust and mechanism studies performed in the aqueous phase are persuasive to some extent.

Our preliminary sulfate quantification results (Fig. 2a and b) suggest that the presence of (bi)carbonate ions under solar light contributes to increased sulfate yield. In this carbonate-containing reaction system, a plausible intermediate is the active $CO_3^{\cdot-}$. It is readily produced via the following two pathways. First of all, carbonate anion can be directly oxidized by produced photo-induced holes from typical mineral dust upon solar irradiation (**R1** and **R2**), as the redox potential of $CO_3^{\cdot-}/CO_3^{2-}$ is 1.78 V (vs NHE, at pH = 7), which is lower than the TiO_2 valence band (VB) potential of 2.67 V (vs NHE, at pH = 7) (Li et al., 2016; Xiong et al., 2016):

$$\text{Mineral dust} + h\nu \rightarrow h^+ + e^- \quad [\mathbf{R1}]$$

$$h^+ + CO_3^{2-} \rightarrow CO_3^{\cdot-} \quad [\mathbf{R2}]$$

In the second pathway, carbonate radicals evolve through the reaction of (bi)carbonate anion with formed hydroxyl radicals ·OH over mineral dust surfaces (Zhang et al., 2015a) (**R3** and **R4**).

$$h^+ + H_2O_{ad} \rightarrow \cdot OH + H^+ \quad [\mathbf{R3}]$$

$$\cdot OH + HCO_3^-/CO_3^{2-} \rightarrow CO_3^{\cdot-} + H_2O/OH^- \quad [\mathbf{R4}]$$

The above assumptions are supported by nanosecond transient absorption spectra (NTAS), in which signal (ΔOD) of carbonate radical $CO_3^{\cdot-}$ at 600 nm (Bhattacharya et al., 1998) only emerges for dust suspension containing (bi)carbonate species (Fig. 7a). An increased degradation rate of aniline observed in TiO_2 suspension due to the presence of carbonate ions produces additional evidence of the formation of active $CO_3^{\cdot-}$ ions and strengthened oxidation capability of TiO_2 (Fig. 7b, see additional discussion in supplementary text 19). The $CO_3^{\cdot-}$-induced chemistry was further evidenced by ·OH scavenging experiments using tertiary Butyl Alcohol (TBA) and isopropanol (i-PrOH) as they show lower reaction rates with $CO_3^{\cdot-}$ ($k_{CO_3^{\cdot-},\text{i-PrOH}} < 4.0 \times 10^4$ M^{-1} s^{-1} and $k_{CO_3^{\cdot-},\text{TBA}} < 1.6 \times 10^2$ M^{-1} s^{-1}) relative to that with ·OH ($k_{\text{i-PrOH}\sim\cdot OH} < 1.9 \times 10^9$ M^{-1} s^{-1} and ($k_{\cdot OH,\text{TBA}} = 6 \times 10^8$ M^{-1} s^{-1}) (Buxton et al., 2009; Liu et al., 2015) (Liu et al., 2015) (Li et al., 2020). TBA dramatically decreases the yield of sulfate on TiO_2 surface by nearly 70 %, with sulfite ions being the dominant sulfur species (Fig. 7c). Meanwhile, a great loss of sulfate yield when TiO_2 suspension was added with i-PrOH (Fig. 7d). This is in strong contrast to the result of a carbonate-involved system where the reactivity is sustained as carbonate radicals offer an alternative reaction pathway for SO_2 oxidation. This is plausible since the carbonate ions are excellent ·OH scavenger, and $CO_3^{\cdot-}$ becomes the predominant species in a relatively strong alkaline aqueous-like environment in the presence of carbonate salt. This is supported by the previous work (Sun et al., 2016), in which adding 0.1 M of bicarbonate salt into the UV/H_2O_2 system (H_2O_2 = 0.3 mM) was sufficient to suppress ·OH concentration to around 10^{-15} M, creating a carbonate radical dominated regime ($[CO_3^{\cdot-}] = 8.64 \times 10^{-12}$ M). In our experiments (Fig. 7b), 0.2 M of carbonate salt was employed, and the reaction rate of CO_3^{2-} with ·OH is nearly two orders of magnitude higher than that of HCO_3^-, thus giving rise to carbonate radical being the substitute for hydroxyl radical in the reaction. The above results suggest that ·OH is a major contributor to sulfate yield on TiO_2 particles in the absence of carbonate ions while $CO_3^{\cdot-}$ ions dominate SO_2 oxidation over humidfied carbonate-containing TiO_2 particles upon irradiation. In addition to experimental investigations, the carbonate radical formation process is proved to be thermodynamically favorable, supported by density functional theory (DFT) calculations (Fig. S10 and supplementary text 20).

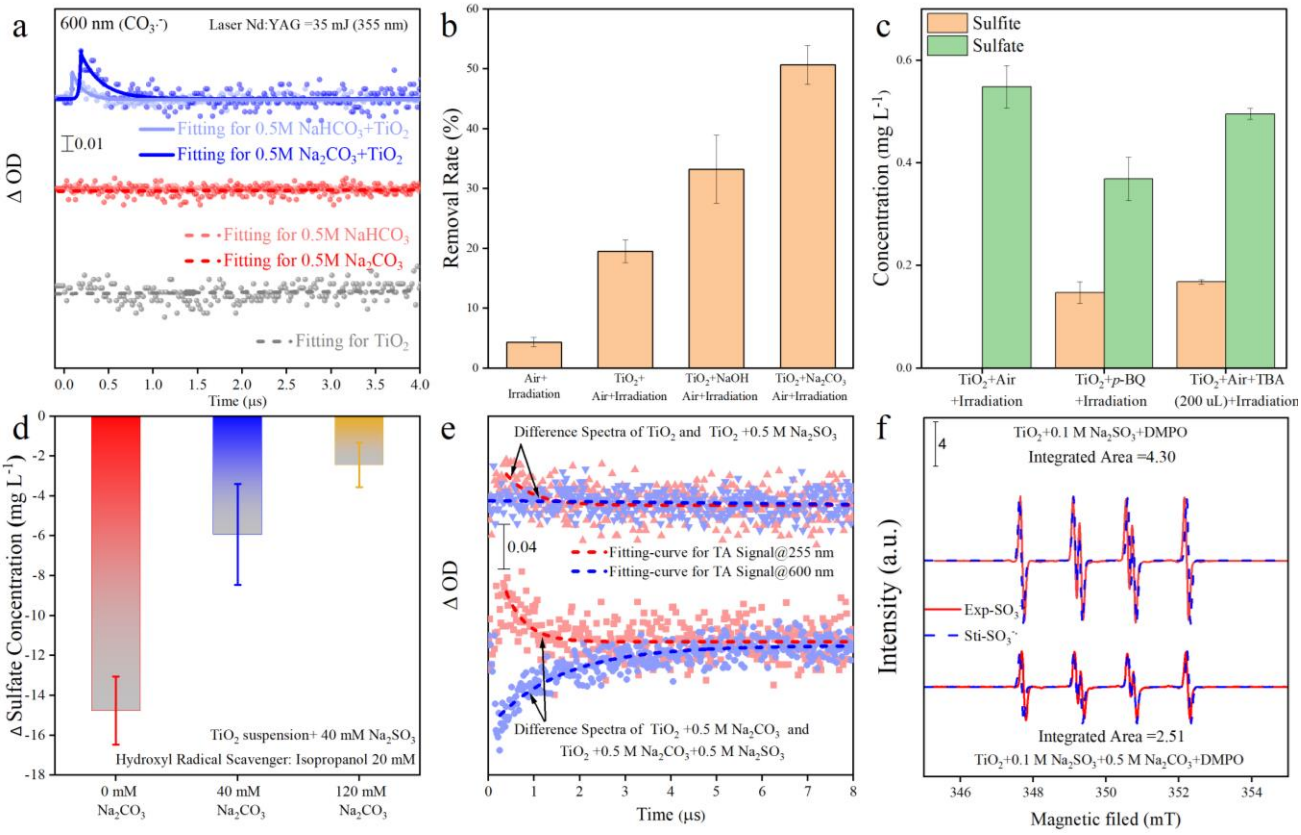

Figure 7. (**a**) Single-wavelength transient absorption spectra of various aqueous solutions. (**b**) The removal rate of aniline after exposure to airflow under irradiation in the absence and presence of mineral dust particles for 300 seconds. Reaction conditions: RH = 30 %, Light intensity (I) = 30 mW cm^{-2}, Total flow rate = 52.5 mL min^{-1}. Noting that an adequate amount of NaOH was introduced into the TiO_2 suspension system to achieve a pH environment condition identical to that of the TiO_2+Na_2CO_3 suspension system. (**c**) Determination of sulfite and sulfate concentration after exposure to air flow under irradiation in the absence and presence of mineral dust particles for 20 min. Reaction conditions: RH = 30 %, Light intensity (I) = 30 mW cm^{-2}, Total flow rate = 52.5 mL min^{-1}. (**d**) Sulfate formation change $\Delta(SO_4^{2-})$ is determined by different sulfate concentrations with and without the addition of isopropanol as hydroxyl radical scavenger. (**e**) The difference in transient absorption kinetics of sulfite radical and carbonate radical at the various aqueous solutions and their corresponding growth-decay fit curves. ΔA-signal was recorded at 255 and 600 nm after pulsed 355 nm laser excitation. (**f**) ESR spectrometry of [DMPO–$SO_3^{\cdot-}$] intermediate formed in a solution of d TiO_2 (3 mg~4 mL) + 0.1 M Na_2SO_3 and TiO_2 (3 mg~4 mL) + 0.5 M Na_2CO_3 + 0.1 M Na_2SO_3. For clarity, the integrated areas of ESR profiles were also presented for direct comparison. Exp. and Sti. stand for experimental results and corresponding fitting results using software Isotropic Radicals.

On the other hand, early studies (Chameides and Davis, 1982; Das, 2001; Neta and Huie, 1985) agree with the key role of sulfite radical ($SO_3^{\cdot-}$) in rapid sulfate production in an aqueous medium, and the present reaction system creates a localized environment where $SO_3^{\cdot-}$ can be readily produced from the TiO_2 and S(IV) species upon solar illumination (Salama et al., 1995). Consequently, probe light of NTAS at wavelength 255 nm (ascribed to sulfite radical) and 600 nm (ascribed to carbonate

radical) were simultaneously monitored (Ghalei et al., 2016; Goldstein et al., 2001; Hayon et al., 1972). A weak signal of sulfite radical was observed in the system of TiO_2+Na_2SO_3 suspension under irradiation (Fig. 7e). On the contrary, the sulfite radical signal is strengthened after the introduction of carbonate ions into the TiO_2+Na_2SO_3 suspension, along with a significant decrease in the signal for carbonate radical. Electron spin resonance (ESR) data (Fig. 7f) further confirms the increase of $SO_3^{\cdot-}$ after 2 min UV irradiation in the presence of carbonate ion. Based on the above results, one may deduce that the interplay between carbonate radical and sulfite ions is a crucial step giving rise to the increased $SO_3^{\cdot-}$, which is reported to account for rapid atmospheric sulfate formation through chain propagation reactions that involve $SO_4^{\cdot-}$ and $SO_5^{\cdot-}$ intermediates (Hung and Hoffmann, 2015; Hung et al., 2018). Additionally, this sulfite radical ion chemistry is believed to drive fast sulfate formation over mineral dust particles as well (Gankanda et al., 2016; Rubasinghege et al., 2010). Nevertheless, there are two possibilities that might explain the aforementioned interaction. One way is the oxygen transfer and the other route is electron transfer, which needs further clarification.

We first examined the oxygen transfer path through ^{18}O isotope labeling experiments. TiO_2 particles were initially exposed to $C^{16}O_2/N_2$ and $C^{18}O_2/N_2$, followed by the exposure of SO_2/N_2+O_2 under irradiation (Fig. 8a). Bidentate carbonate band centered at 1573 cm^{-1} appears after the introduction of $C^{16}O_2/N_2$, while this band shifts to 1558 cm^{-1} when $C^{18}O_2/N_2$ is introduced, indicating the incorporation of ^{18}O into bidentate carbonate species, in accord with the previous report (Liao et al., 2002). However, no shift of IR features at 1269, 1219, and 1159 cm^{-1}, assigned to (bi)sulfate species on TiO_2 particles, were observed throughout the reaction. This implies that the oxygen transfer path does not account for the rapid SO_2 oxidation on particles of concern.

In light of the above analysis, the electron transfer might be a plausible pathway to explain the fast oxidation within the reaction system. DFT calculations provide an accessible approach to study the electron transfer pathway. The result in Fig. 8b illustrates $SO_3^{\cdot-}$ formation is a SET process of $CO_3^{\cdot-}$ and SO_3^{2-}, where O atom in SO_3^{2-} transfers an electron to O atom in $CO_3^{\cdot-}$ to form $SO_3^{\cdot-}$ and CO_3^{2-}. This SET reaction is a thermodynamically favorable process, with the difference of Gibbs free energy between reactant and product lying at -24.09 kcal mol^{-1}. We note that the insufficient O_2 supply in aqueous media may be an underlying constraint to the proposed $CO_3^{\cdot-}$-initiated SO_2 oxidation pathway. Therefore, careful estimation of both oxygen consumption and supply rates were conducted, with results revealing that oxygen supply flux can be sufficiently larger than corresponding consumption (see additional details in the supplementary text 21), allowing us to deduce that considered chain reactions can continually proceed. Taken above results and discussions altogether, the following reactions are proposed accordingly (**R5-R8**):

$$CO_3^{\cdot-} + SO_3^{2-} \rightarrow CO_3^{2-} + SO_3^{\cdot-} \quad [\mathbf{R5}]$$

$$SO_3^{\cdot-} + O_2 \rightarrow SO_5^{\cdot-} \quad [\mathbf{R6}]$$

$$SO_5^{\cdot-} + SO_3^{2-} \rightarrow SO_4^{\cdot-} + SO_4^{2-} \quad [\mathbf{R7}]$$

$$SO_4^{\cdot-} + SO_3^{2-} \rightarrow SO_4^{2-} + SO_3^{\cdot-} \quad [\mathbf{R8}]$$

Another important pathway needs to be considered as well; that is $SO_3^{\cdot-}$ can also be formed via the conventional reaction of ·OH and SO_3^{2-} (**R9**).

$$\cdot OH + SO_3^{2-} \rightarrow SO_3^{\cdot-} + OH^- \quad [\mathbf{R9}]$$

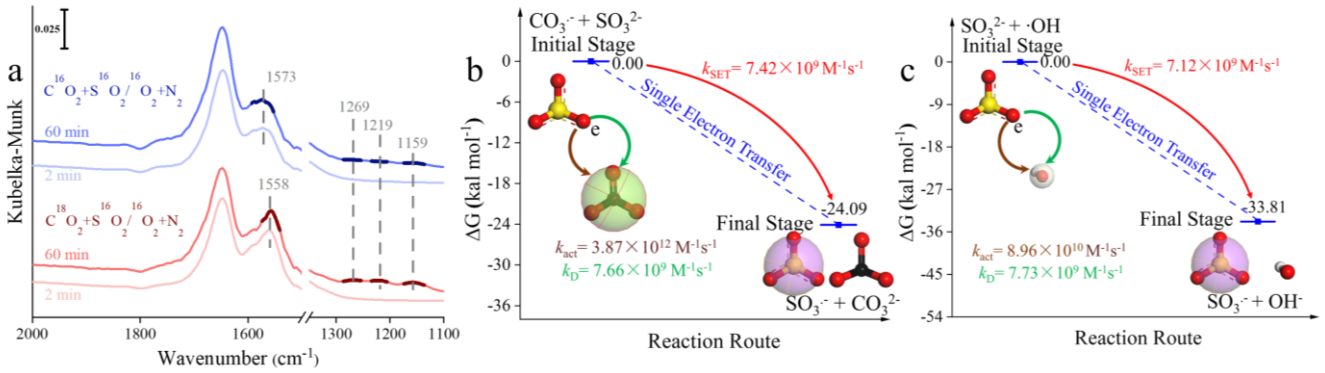

Figure 8. (**a**) *In situ* DRIFTS of heterogeneous reaction of SO_2 on the TiO_2 particles for 2 and 60 min after being exposed to $C^{16(18)}O_2/N_2$ for 20 min under irradiation. (**b**) Reaction pathway of interaction between carbonate radical ($CO_3^{\cdot-}$) and sulfite (SO_3^{2-}) and (**c**) Interaction between hydroxyl radical (·OH) and sulfite (SO_3^{2-}) through the SET process at the CCSD (T)-F12/cc-PVDZ-F12//M06-2X/6-311++G (3df, 3pd) level and ΔG_0^{SET} represents the difference in Gibbs free energy between reactant and product. The white, black, yellow, and red spheres represent H, C, S, and O atoms, respectively. In order to visualize the variation of surface products in oxygen isotope experiments (panel a), DRIFTS features of these concerned species were highlighted in dark colors. For interpretation of the references to color in the legends of panels b and c, the reader is referred to the Web version of this article.

In this SET process, electron donor SO_3^{2-} reacts spontaneously with electron acceptor ·OH (Fig. 8c) and the calculated activation free energy barrier $\Delta G^{\neq}_{SET}$ for this SET reaction is 2.50 kcal mol^{-1}. Hence, the reaction process of ·OH with SO_3^{2-} is diffusion-controlled, and the total rate constant $k_{SET\text{-}2}$ was calculated to be 7.12×10^9 M^{-1}s^{-1}. In comparison, the rate constant $k_{SET\text{-}1}$ of the diffusion-controlled SET process for $CO_3^{\cdot-}$ and SO_3^{2-} was estimated to be 7.42×10^9 M^{-1}s^{-1}. Despite a slight net increase of the rate, the distinguishable concentration of $CO_3^{\cdot-}$ and ·OH should also be taken into account for the rate comparison in varied reaction paths. To visualize the difference, relative rates were calculated according to Eq. **12**:

$$r = \frac{v_{CO_3^{\cdot-} + SO_3^{2-}}}{v_{\cdot OH + SO_3^{2-}}} = \frac{k_{SET\text{-}1}[CO_3^{\cdot-}][SO_3^{2-}]}{k_{SET\text{-}2}[\cdot OH][SO_3^{2-}]} \quad [\mathbf{12}]$$

Where *r* is the ratio of two reaction rates, [$CO_3^{\cdot-}$], [SO_3^{2-}], and [·OH] refer to the concentration of corresponding reactants. Previous literature suggests the concentration of carbonate radicals is able to show two orders of magnitude higher than that of hydroxyl radicals at the surface of the water under solar irradiation (Chandrasekaran and Thomas, 1983; Goldstein et al., 2001; Sulzberger et al., 1997), consistent with concentration gap between carbonate radicals and hydroxyl radicals through partitioning process from gas-phase determined in our reaction system (Fig.9). While the net concentrations of carbonate hydroxyl radicals in the water layers of humified particles are very likely to be different from that found in the bulk aqueous

media, concentration inputs of two radicals with the gap of two orders somehow could reflect the relative contribution of carbonate radicals and hydroxyl radicals to sulfate production based on literature results and our experimental trails. The concentrations of $CO_3^{\cdot-}$ and ·OH were set in the range from 1.0×10^{-10} to 1×10^{-12} mol L^{-1} and from 1.0×10^{-12} to 1×10^{-14} mol L^{-1} (Sulzberger et al., 1997) and *r* value could thus reach to 1.04×10^4 at most (Fig. S11). As a result, we speculate that the formation pathway of $SO_3^{\cdot-}$ via interaction between $CO_3^{\cdot-}$ and SO_3^{2-} is a more efficient route, corresponding well with our experimental results.

In addition to the pathway launched by photo-generated holes, the sink of photo-generated electrons is as well considered. In our reaction system, O_2 is thought to be an electron trap and produce the superoxide radical ions ($O_2^{\cdot-}$), which is reported to play a non-negligible role in sulfate formation (Shang et al., 2010) and should be taken into account to give a whole picture of reaction scheme in triggering sulfate formation on the surface of TiO_2-containing mineral dust particles. *p*-benzoquinone is a commonly-used $O_2^{\cdot-}$ scavenger for trapping the $O_2^{\cdot-}$ radical ions (Yan et al., 2018). Our data shows that adding an excess amount of *p*-benzoquinone into TiO_2 particles reduces the sulfate yield by 32 % along with the appearance of sulfite ions over TiO_2 particles upon exposure to SO_2 (Fig.7c). Notably, the decrease in sulfate yield by around 30 % in the presence of $O_2^{\cdot-}$ scavenger *p*-benzoquinone is almost complementary to that added with ·OH scavenger using TBA (70 %), pointing toward a minor sulfate formation pathway contributed by $O_2^{\cdot-}$ relative to the major pathway by $CO_3^{\cdot-}$ when carbonate ions are presented to efficiently capture ·OH ions. Following Shang's work (Shang et al., 2010), $O_2^{\cdot-}$ involved SO_2 oxidation can be given as **R10-R12**:

$$e^- + O_2 \rightarrow O_2^{\cdot-} \quad [\mathbf{R10}]$$

$$SO_2 + O_2^{\cdot-} \rightarrow SO_3 + O^{\cdot-} \quad [\mathbf{R11}]$$

$$SO_3 + H_2O \rightarrow H_2SO_4 \quad [\mathbf{R12}]$$

Where intermediates SO_3 formed via the interaction between SO_2 and $O_2^{\cdot-}$, subsequently couple with water molecules to produce sulfate species as a final product. pH is an important factor within aqueous chemical reaction processes and is in preference to alter the dominated regime for sulfate production. Yet so far adjusting the pH of particle surfaces is quite tough, and exploring the role of dust surface pH in the reactivity of $CO_3^{\cdot-}$ is not easily achieved. Notwithstanding, the increase of pH in TiO_2 suspension was observed to promote the production of $CO_3^{\cdot-}$, further strengthening the oxidation capability of dust particles (Fig. 7b). In contrast, decreasing pH is expected to reduce the yield of $CO_3^{\cdot-}$ since the reaction rate of CO_3^{2-} with ·OH is nearly two orders of magnitude higher than that with HCO_3^-. On this basis, a question arises whether the surface pH of mineral dust can be sustained to maintain fast SO_2 oxidation triggered by $CO_3^{\cdot-}$ in the typical lifespan of mineral dust.

Considering that SO_2 concentration employed in this work is higher than that in the real atmosphere, the concept of "equivalent exposure time" is introduced to evaluate the influence of pH on the SO_2 oxidation pathway initiated by $CO_3^{\cdot-}$ (see a more detailed discussion on determining equivalent exposure time in supplementary text 22). The heterogeneous sulfate production over TiO_2 and TiO_2+$CaCO_3$ particles versus equivalent exposure time were plotted (Fig. S12). Clearly, the sulfate yield builds up steadily during the two-week equivalent exposure time, suggesting that the regime of $CO_3^{\cdot-}$ initiated SO_2

oxidation over TiO_2 and TiO_2+$CaCO_3$ particles is slightly affected by the possible decrease of surface pH because of the accumulation of sulfate production over entire reaction course. In the atmosphere, the lifetime of mineral dust particles ranges from several days to weeks (Bauer and Koch, 2005), and the equivalent exposure time considered in this study (nearly 2 weeks) falls right within the characteristic lifespan range of mineral dust particles. Besides, 20 ppb is assumed to be an atmospherically relevant concentration to calculate "equivalent exposure time" in this study whereas even low SO_2 concentrations (several or a few tens ppb of SO_2) were monitored in the field observation (He et al., 2014; Watanabe et al., 2020). Therefore, the reduction of dust surfaces pH would be more moderate than we now considering and even little influence of surface pH on our proposed reaction scheme would have. This leads us to deduce that persistent growth of sulfate shows a negligible effect on $CO_3^{\cdot-}$ initiated SO_2 oxidation scheme proposed in this work.

Additionally, dust particles are reported to eject the radical ions from the surface under solar light irradiation, severing as an underlying pathway for sulfate aerosol formation in the atmosphere (Chen et al., 2021; Dupart et al., 2012), as described as:

Mineral Dust + $h\nu$ → ROS (g) [**R13**]

ROS (g)+ humidified Air+ SO_2→Sulfate(g) [**R14**]

Where ROS (g) stands for the active intermediates in the gas phase. Over 400 ppm of CO_2 is universal in the atmosphere, and it is expected to form (bi)carbonate ions once enters the quasi-liquid layer of humified particles. Bi(carbonate) ions are then prone to react with hydroxyl radical ions to form carbonate radicals. Following this line of reasoning, we attempt to monitor the plausible gas ROS species that are formed in the presence of CO_2 (see detailed discussion in the experimental section).

When CO_2 (atmospheric relevant concentration) is introduced into the homemade flow-cell chamber, with the intervening gap between TiO_2-coated film and probe molecule solution fixing at nearly 2 mm, the short distance of which guarantees gaseous ROS to diffuse and react with aniline (None, 2013). An increased degradation rate of this probe molecule was seen, which can be speculated to be the generation of active carbonate radical ions (Fig. 9). Aqueous $CO_3^{\cdot-}$ is believed to be supplied by partitioning processes from $CO_3^{\cdot-}$(g) that comes from humified dust particles, and its maximum steady-state concentration was determined to be 1.39×10^{-13} M for "TiO_2+Air+CO_2" system, which is over 1.8 orders of magnitudes higher than that of ·OH for "TiO_2+Air" system (2.15×10^{-15} M). This observation matches with the early study where the concentration of carbonate radical can be nearly two orders of magnitudes than ·OH over the water surface (Sulzberger et al., 1997).

Overall, the above results suggest that the photochemistry that involves carbonate ions, more precisely $CO_3^{\cdot-}$ radicals, increases sulfate production. This finding broadens the prevailing view that acceleration of SO_2 oxidation over the carbonate salt is merely due to the favorable neutralization of H_2SO_4 over an alkaline surface. To be important, upon irradiation active component TiO_2 in mineral dust produce carbonate radicals in the gas phase when CO_2 presents, therefore potentially promoting sulfate aerosol formation in the atmosphere. Overall, it could be speculated that (bi)carbonate species strengthen the oxidative capacity of TiO_2-containing dust particles with regard to SO_2 oxidation.

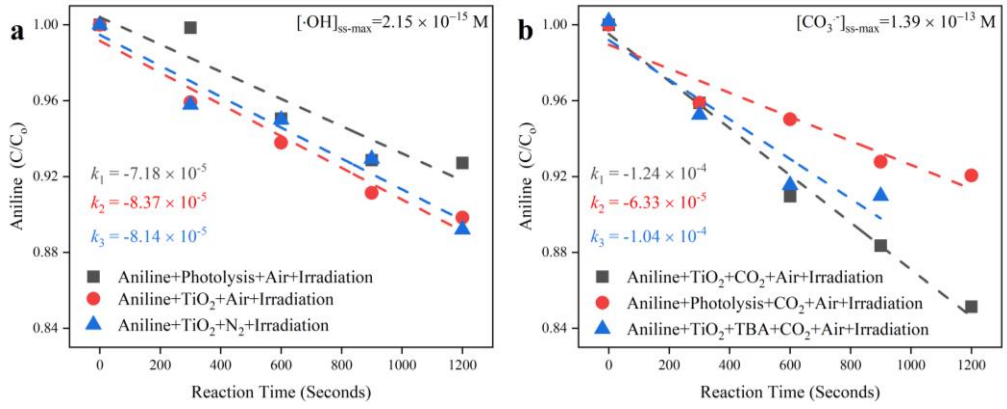

Figure 9. The degradation rate of aniline after exposure to air flow under irradiation in the absence **(a)** and presence **(b)** of CO_2 over mineral dust proxy particles TiO_2 as function of the reaction time. Reaction conditions: RH = 30 %, Light intensity (I) = 30 mW cm^{-2}, Total flow rate = 52.5 mL min^{-1}.

3.2.4 Field Measurements of Sulfate and (Bi)carbonate Ions.

Complement field sampling and analysis were further conducted to examine our hypothesis that intermediates $CO_3^{\cdot-}$ may play role in secondary sulfate formation in the atmosphere. We first considered the meteorological condition wind speed, which is an important parameter determining whether the local chemical process gains importance in affecting secondary sulfate formation. Meteorological information was collected from the open-access database (https://www.aqistudy.cn/). During the sampling period, the wind scale mainly varies from 0 to 1, corresponding to the wind speed ranging from 0 to 1.5 m s^{-1} (Fig. S13). All plots shown in Fig. S13 give rise to a statistical wind speed of 0.76 ± 0.73, which represents the weak dispersion of pollutants at low wind speed (not exceeding 2.5 m s^{-1})(Liu et al., 2020a; Witkowska et al., 2016), indicating that local source is a dominant contributor to the air pollution.

Under stagnant meteorological conditions (wind speed < 1.5 m s^{-1}), for the coarse-mode (2.5 μm ~ 10 μm) of sulfate, the heterogeneous reaction of SO_2 on the dust surfaces is thought to be a major contributor (Liu et al., 2017). This correlates to the fact that a large mass fraction of mineral dust is abundant in coarse-model particulate matter (PM) (Fang et al., 2017; Miller-Schulze et al., 2015), in which TiO_2 was found at mass mixing ratios ranging from 0.1 to 10 % depending on the exact location where particles were uplifted (Chen et al., 2012; Hanisch and Crowley, 2003). Therefore, PM with relatively larger size dimensions is expected to contribute to secondary sulfate formation via heterogeneous reactions, which is supported by the recent field study where the carbonate fraction of coarse PM is evidenced to promote secondary sulfate production (Song et al., 2018). Considering this, rather than determining the concentration of water-soluble ions in all stages, special attention is focused on PM collected in stages 1-4 (particles with their dimension $\geqslant$ 3.3 μm). As (bi)carbonate ions are known as key precursors in producing $CO_3^{\cdot-}$ and accelerating sulfate formation, quantifications of those relevant water-soluble ions were thus conducted (see details in the experimental section and supplementary text 13).

We further consider the relationships between sulfate ions and (bi)carbonate ions by means of linear regression analysis. However, under the low wind speed (0.76 ± 0.73), correlation coefficients R^2 obtained for the relationship between bi(carbonate) and sulfate ions are not promising, 0.56 (sulfate vs carbonate) and 0.61 (sulfate vs bicarbonate) for $PM_{3.3}$-$PM_{9.0}$ during daytime hours (Fig. 10). A plausible explanation is that in spite of little significance, local primary emission source also brings bias and uncertainty to the correlation results. Shanghai is a coastal city, and sulfate species such as K_2SO_4 and Na_2SO_4 from the sea salt contribute to the local sulfate emission as well (Long et al., 2014). On the other hand, this novel SO_2 oxidation channel is yet to be in the infant stage, and only active mineral dust components have been considered in this work whereas other components found in the coarse mode of PM such as organic matter, elemental carbon as well as sea salt (Cheung et al., 2011) are likely to involve this mechanism and alter the response of sulfate yield to SO_2 heterogeneous uptake. In addition, the water-soluble ions determined in these samples may not come from the net contribution of heterogenous reaction processes in absolute daytime and nighttime periods. In other words, some of the collected samples, experiencing heterogeneous reaction that occurs during day(nigh)-night(day) shifts periods, inevitably being assigned to the sulfate ions measured in separate sampling hours, thus reducing the correlation coefficients.

For those large particles (LP), which refer to the particles with a diameter large than 9 μm in this work, sulfate ions show a rather weak or even no correlation to (bi)carbonate ions during the nighttime and day-time hours (Fig. S14). This is likely due to the short lifetime of LP. Generally, the aerosol lifetime is on the order of less than an hour to days (Koelemeijer et al., 2006), highly depending on particle size. For example, the lifetime of PM_{10} ranges from minutes to hours, and its travel distance, in general, is less than 10 km (Agustine et al., 2018). As a consequence, secondary sulfate formation through chemical reaction over LP is not significant with respect to *in situ* emissions. When PM downsizes to 2.5 μm, $PM_{2.5}$ has a lifetime prolonged to nearly one day or longer (Wu et al., 2020). Therefore, $PM_{3.3}$-$PM_{9.0}$ are expected to have a relatively long lifetime, on the order of several hours on average, which enables the heterogeneous reaction process to become a more important contributor to overall sulfate measured in $PM_{3.3}$-$PM_{9.0}$ than that in $PM_{\geq 9.0}$. This is supported by our observations where during the daytime hours the correlation coefficients for $PM_{3.3}$-$PM_{9.0}$, i.e. 0.56 (sulfate vs carbonate) and 0.61 (sulfate vs bicarbonate), are higher than that of $PM_{\geq 9.0}$, i.e. 0.489 (sulfate vs carbonate) and 0.36 (sulfate vs bicarbonate), respectively. Likewise, higher correlation coefficients are also observed for $PM_{3.3}$-$PM_{9.0}$ than $PM_{\geq 9.0}$ in the sample collected during the nighttime periods.

While we note that the correlations between sulfate and (bi)carbonate are not high in this work, ground-based field measurements of sulfate and (bi)carbonate ions shed light on their distinct correlations during the daytime and nighttime hours. In Fig. 10 and Fig. S14, the negative correlations between the mass concentrations of sulfate ions and (bi)carbonate ions are observed in the nighttime hours, consistent with the suppression of sulfate formation by CO_2 in the dark experiments. This is also supported by lab-based observations where CO_2-derived (bi)carbonate species are demonstrated to suppress sulfate production over two dominant mineral dust components aluminum oxide (Liu et al., 2020c) and silicon dioxide (Fig. S15 and supplementary text 23). Alternatively, while CO_2-derived (bi)carbonate may slightly affect sulfate accumulation over PM with high water content in the dark scenario, fresh PM is usually dry when emitted into the atmosphere. Due to the competitive

adsorption, the occurrence of suppression of SO_2 adsorption and subsequent sulfate formation is possible in the early emission stage before PM becomes wet, thus contributing to the overall negative correlation.

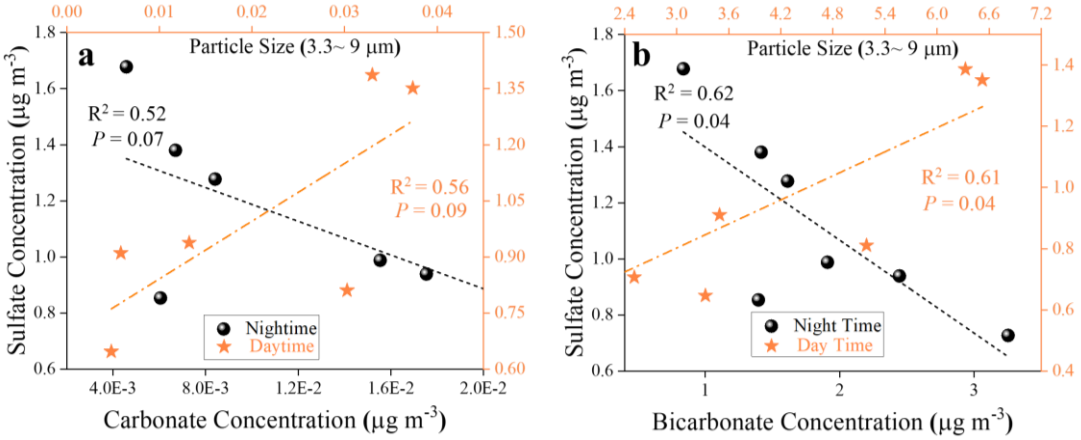

Figure 10. Field observation for the relationship between carbonate and sulfate ions during daytime and night-time hours. Linear relationship analyses for measured sulfate ions and estimated carbonate ions (**a**) and for measured sulfate ions and estimated bicarbonate ions (**b**) during the daytime and night-time hours, with particle sizes of PM ranging from 3.3 to 9 μm.

Instead, positive correlations were seen for those ions within PM sampled during the daytime hours regardless of size ranges and carbonate types (HCO_3^-/CO_3^{2-}). This matches with the scenarios in which sulfate production upon irradiation in the presence of (bi) carbonate ions is increased over both model and authentic dust particles. Except the case (nighttime period, size larger than 9 μm), most of the significance *P* values for their correlations were smaller than 0.1, specifically with significance *P* values below 0.5 determined for bicarbonate vs sulfate, implying the plausible underlying connection between sulfate and (bi)carbonate ions. In fact, preceding ground-based observations of a highly correlated relationship between Ca^{2+} and SO_4^{2-} water-soluble ions (Wu et al., 2020) during the carbonate-enriched dust storm episodes, together with persistent reports on the significant role of photochemical channels in elevating the sulfate concentration level during the daytime hours (Kim et al., 2017; Wei et al., 2019; Wu et al., 2017) indirectly reflects the possibility of accelerated SO_2 oxidation triggered by photo-generated active intermediates associated with carbonate species.

Overall, this is the first time that relationships between those ions are explored separately in these two periods. Taken together, carbonate radical is likely to promote sulfate production in the atmosphere during daytime hours. Detailed and systematic SO_2 oxidation channel triggered by $CO_3^{\cdot-}$ needs further investigations to enable a better interpretation of correlations between these inorganic ions at the given meteorological conditions of sampling and physicochemical properties of PM.

4. Conclusion

On the basis of the experimental and theoretical results derived from this work, we for the first time propose a novel reaction channel for fast SO_2 oxidation over mineral dust particles due to the formation of carbonate radical ions. A schematic chart for

the sulfate formation in the presence of carbonate radicals upon solar light or bi(carbonate) ions under dark conditions is summarized and elucidated in Fig. 11. During the nighttime hours at 298 K (ambient temperature) CO_2-derived (bi)carbonate species are prone to have a slightly negative effect on sulfate formation presumably due to the competitive adsorption between CO_2 and SO_2. For alkaline carbonate salt, it favors sulfate formation through the neutralization process. On the other hand, in the daytime, both CO_2-derived (bi)carbonate species and carbonate salt work as the precursor of $CO_3^{\cdot-}$, which promotes sulfate formation. Especially, uptake coefficients for carbonate salt containing mineral dust can be increased by 17 times, which is more pronounced than the increase due to the neutralization regime in the dark condition. Consistent with the findings reported in the early studies (Chen et al., 2021; Dupart et al., 2012), we speculate the production of gas-phase $CO_3^{\cdot}$ ions when mineral dust particles are irradiated in the presence of CO_2 (atmospherically relevant concentration 400 ppm). This observation potentially implies that the increased sulfate yield in part comes from increased external secondary sulfate aerosol triggered by $CO_3^{\cdot-}$ (g).

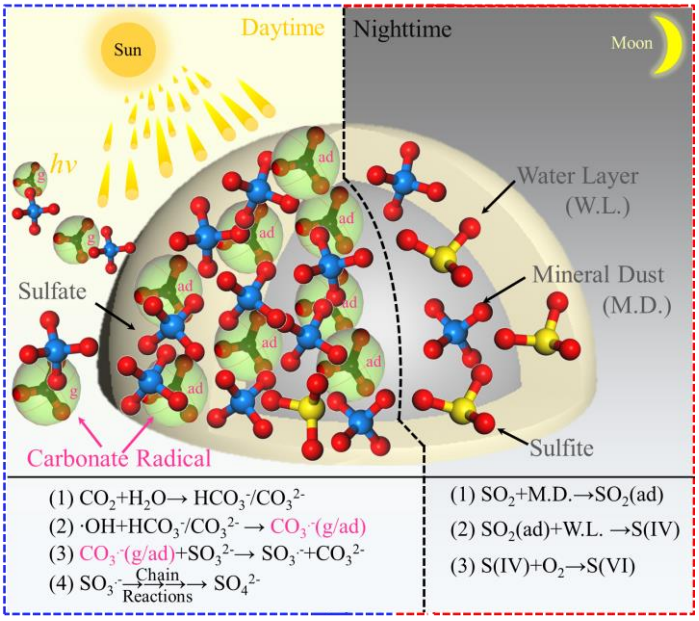

Figure 11. Schematic of the sulfate formation in the presence and absence of carbonate radical. Noting that g and ad represent gas-phase and adsorbed carbonate radical ions, respectively.

By means of ROS scavenger experiments, direct observation of carbonate radical using NTAS analysis, oxygen isotope assay, ESR measurement as well as DFT calculations, $CO_3^{\cdot-}$-initiated S(IV) oxidation involving single electron transfer process are elucidated. While carbonate radical ions are mainly responsible for rapid sulfate formation, superoxide radical ions are likely to serve as a minor pathway over TiO_2-containing mineral dust particles (not shown on the schematic chart to direct readers' focus on $CO_3^{\cdot-}$). In addition, a weak correlation between sulfate ions and (bi)carbonate ions observed for $PM_{3.3}$-$PM_{9.0}$ in this work reasonably correlates to non-chemical primary emission and the complicated nature of $CO_3^{\cdot-}$ regime of sulfate

production in the atmosphere. Nonetheless, complement field sampling of ambient PM and analysis of sulfate and (bi)carbonate ions in this study unfold their distinct correlations during the daytime and nighttime hours, these two tendencies of which agree with the experimental observations.

In this work, only atmospheric secondary sulfate formation was considered, whereas the oxidation of primary organic species yet has not been investigated. In fact, carbonate radical ions are prone to rapidly react with electron-rich organics amines (Stenman et al., 2003; Yan et al., 2019) as well as phenol (Busset et al., 2007; Xiong et al., 2016), and it may potentially serve as the key oxidants that drive the fast formation of SOA in the atmosphere. Besides, observation of strengthened photochemistry launched by carbonate radicals suggests that such chemistry may be amplified on atmospherically relevant reactions that occur in cloud droplets as well as fog water where they often contain hydroxyl radicals and water-soluble (bi)carbonate ions.

To be important, gas-phase carbonate radical ions are speculated to be formed in the atmospherically relevant CO_2 concentration (400 ppm) when mineral dust is irradiated. This will help the formation of external sulfate aerosol formation. Since both sulfate aerosol and CO_2 are well known to regulate the radiation budget and solar energy balance on the earth (Cheung et al., 2011; Möller, 1964), coupled with the CO_2-intiated promoted sulfate pathway found here, their overall influence on the global climate needs further investigation. Therefore, our study highlights the necessity for a comprehensive understanding of the $CO_3^{\cdot-}$ relevant chemistry in the underlying impacts of fine PM concentration, human health, and climate. All these assumptions need to be investigated in further detail. This study provides the indication that carbonate radical not only plays a role as a marginal intermediate in tropospheric anion chemistry but also as a strong oxidant for surfacial processing of trace gas in the atmosphere.

Data availability. The data that support the results are available from the corresponding author upon request.

Author contributions. Y.L., Y.D. and L.Z. initially proposed the idea; Y.L. and Y.D. together designed the experiments, and Y.L. performed the most of the experiments; J.L. performed DFT calculations; Y.L., X.Z. and T.W. contributed to field samplings and data analysis; K.L., K.G., A.B., I.N., Q.G., X.Z., C.G., and L.Z. provided suggestions on the experiments and paper writing; All authors wrote the manuscript.

Competing interests. The authors declare that they have no conflict of interest.

Acknowledgements. We greatly appreciate Dr. Yang Yang and Prof. Keli Han from Dalian institute of chemical physics for NTAS and some helpful discussions.

Financial support. This work was supported by the National Natural Science Foundation of China (No. 21976030 and No. 21677037), National key research and development program of China (2016YFE0112200 and 2016YFC0202700), the Natural Science Foundation of Shanghai (No. 19ZR1471200 and No. 17ZR1440200).

References

Abou-Ghanem M, Oliynyk AO, Chen ZH, Matchett LC, McGrath DT, Katz MJ, et al.: Significant Variability in the Photocatalytic Activity of Natural Titanium-Containing Minerals: Implications for Understanding and Predicting Atmospheric Mineral Dust Photochemistry. Environ. Sci. Technol., 54,13509-13516, https://doi.org/10.1021/acs.est.0c05861, 2020.

Agustine I, Yulinawati H, Gunawan D, Suswantoro E: Potential impact of particulate matter less than 10 micron (PM_{10}) to ambient air quality of Jakarta and Palembang. Iop C Ser Earth Env, 106,012057, https://doi.org/10.1088/1755-1315/106/1/012057, 2018.

Al-Hosney HA, Grassian VH: Water, sulfur dioxide and nitric acid adsorption on calcium carbonate: A transmission and ATR-FTIR study. Phys. Chem. Chem. Phys., 7,1266-1276, https://doi.org/10.1039/b417872f, 2005.

Al-Salihi AM, Mohammed TH: The effect of dust storms on some meteorological elements over Baghdad , Iraq: Study Cases. IOSR Journal of Applied Physics, 7,Ver. II PP 01-07, https://doi.org/10.9790/4861-07220107, 2015.

Balachandran U, Eror NG: Raman-Spectra Of Titanium-Dioxide. J. Solid State Chem., 42,276-282, https://doi.org/10.1016/0022-4596(82)90006-8, 1982.

Baltrusaitis J, Schuttlefield J, Zeitler E, Grassian VH: Carbon dioxide adsorption on oxide nanoparticle surfaces. Chem. Eng. J., 170,471-481, https://doi.org/10.1016/j.cej.2010.12.041, 2011.

Bao H, Yu S, Tong DQ: Massive volcanic SO_2 oxidation and sulphate aerosol deposition in Cenozoic North America. Nature, 465,909-912, https://doi.org/10.1038/nature09100, 2010.

Bauer SE, Koch D: Impact of heterogeneous sulfate formation at mineral dust surfaces on aerosol loads and radiative forcing in the Goddard Institute for Space Studies general circulation model. J. Geophys. Res., 110,D17202, https://doi.org/10.1029/2005jd005870, 2005.

Behrman EJ: Degradation kinetics and mechanism of aniline by heat-assisted persulfate oxidation Comment. J. Environ. Sci. China, 64,352-352, https://doi.org/10.1016/j.jes.2018.02.008, 2018.

Beig G, Brasseur GP: Model of tropospheric ion composition: A first attempt. J. Geophys. Res., 105,22671-22684, https://doi.org/10.1029/2000JD900119, 2000.

Bhattacharya A, Amitabha D, Mandal PC: Carbonate radical induced polymerisation of pyrrole: A steady state and flash photolysis study. J. Radioanal Nucl. Ch., 230,91-95, https://doi.org/10.1007/BF02387452, 1998.

Bisby RH, Johnson SA, Parker AW, Tavender SM: Time-resolved resonance Raman spectroscopy of the carbonate radical. J. Chem. Soc. Faraday Trans., 94,2069-2072, https://doi.org/10.1039/A801239C, 1998.

Busset C, Mazellier P, Sarakha M, De Laat J: Photochemical generation of carbonate radicals and their reactivity with phenol. J. Photoch. Photobio. A, 185,127-132, https://doi.org/10.1016/j.jphotochem.2006.04.045, 2007.

Buxton GV, Greenstock CL, Helman WP, Ross AB: Critical Review of rate constants for reactions of hydrated electrons, hydrogen atoms and hydroxyl radicals ($\cdot OH/\cdot O^-$ in aqueous solution. J. Phys. Chem. Ref. Data, 17,513-886, https://doi.org/10.1063/1.555805, 2009.

Cao JJ, Lee SC, Zhang XY, Chow JC, An ZS, Ho KF, et al.: Characterization of airborne carbonate over a site near Asian dust source regions during spring 2002 and its climatic and environmental significance. J. Geophys. Res., 110,1-8, https://doi.org/10.1029/2004JD005244, 2005.

Chameides WL, Davis DD: The Free-Radical chemistry of cloud droplets and its impact upon the composition of rain. J. Geophs Res. Oceans, 87,4863-4877, https://doi.org/10.1029/JC087iC07p04863, 1982.

Chandrasekaran K, Thomas JK: Photochemical reduction of carbonate to formaldehyde on TiO_2 powder. Chem. Phys. Lett., 99,7-10, https://doi.org/10.1016/0009-2614(83)80259-0, 1983.

Chen HH, Nanayakkara CE, Grassian VH: Titanium Dioxide Photocatalysis in Atmospheric Chemistry. Chem. Rev., 112,5919-5948, https://doi.org/10.1021/cr3002092, 2012.

Chen Y, Tong SR, Li WR, Liu YP, Tan F, Ge MF, et al.: Photocatalytic Oxidation of SO_2 by TiO_2: Aerosol Formation and the Key Role of Gaseous Reactive Oxygen Species. Environ. Sci. Technol., 55,9784-9793, https://doi.org/10.1021/acs.est.1c01608, 2021.

Cheung K, Daher N, Kam W, Shafer MM, Ning Z, Schauer JJ, et al.: Spatial and temporal variation of chemical composition and mass closure of ambient coarse particulate matter ($PM_{10-2.5}$) in the Los Angeles area. Atmos. Environ., 45,2651-2662, https://doi.org/10.1016/j.atmosenv.2011.02.066, 2011.

Cope VW, Chen S-N, Hoffman MZ: Intermediates in the photochemistry of of carbonato-amine complexes of cobalt(III). carbonate(-) radicals and the aquocarbonato complex. J. Am. Chem. Soc., 95,3116-3121, https://doi.org/10.1021/ja00791a005, 1973

Csavina J, Field J, Felix O, Corral-Avitia AY, Saez AE, Betterton EA: Effect of wind speed and relative humidity on atmospheric dust concentrations in semi-arid climates. Sci.Total. Envrion., 487,82-90, https://doi.org/10.1016/j.scitotenv.2014.03.138, 2014.

Cwiertny DM, Young MA, Grassian VH: Chemistry and photochemistry of mineral dust aerosol. Annu. Rev. Phys. Chem., 59,27-51, https://doi.org/10.1146/annurev.physchem.59.032607.093630, 2008.

Das TN: Reactivity and role of SO_5.- radical in aqueous medium chain oxidation of sulfite to sulfate and atmospheric sulfuric acid generation. J. Phys. Chem. A, 105,9142-9155, https://doi.org/10.1021/jp011255h, 2001.

Deng Y, Liu Y, Wang T, Cheng H, Feng Y, Yang Y, et al.: Photochemical reaction of CO_2 on atmospheric mineral dusts. Atmos. Environ., 223,117222.1-117222.10, https://doi.org/10.1016/j.atmosenv.2019.117222, 2020.

Dong XY, Fu JS, Huang K, Tong D, Zhuang GS: Model development of dust emission and heterogeneous chemistry within the Community Multiscale Air Quality modeling system and its application over East Asia. Atmos. Chem. Phys., 16,8157-8180, https://doi.org/10.5194/acp-16-8157-2016, 2016.

Dupart Y, King SM, Nekat B, Nowak A, Wiedensohler A, Herrmann H, et al.: Mineral dust photochemistry induces nucleation events in the presence of SO_2. Proc. Natl. Acad. Sci. USA, 109,20842-20847, https://doi.org/10.1073/pnas.1212297109, 2012.

Duran A, Monteagudo JM, Martin IS, Merino S, Chen X, Shi X: Solar photo-degradation of aniline with rGO/TiO_2 composites and persulfate. Sci.Total. Envrion., 697,134086-, https://doi.org/10.1016/j.scitotenv.2019.134086, 2019.

El Zein A, Romanias MN, Bedjanian Y: Kinetics and Products of Heterogeneous Reaction of HONO with Fe_2O_3 and Arizona Test Dust. Environ. Sci. Technol., 47,6325-6331, https://doi.org/10.1021/es400794c, 2013.

Ervens B, George C, Williams JE, Buxton GV, Salmon GA, Bydder M, et al.: CAPRAM 2.4 (MODAC mechanism): An extended and condensed tropospheric aqueous phase mechanism and its application. J. Geophys. Res., 108,4426, https://doi.org/10.1029/2002jd002202, 2003.

Fang T, Guo H, Zeng L, Verma V, Nenes A, Weber RJ: Highly Acidic Ambient Particles, Soluble Metals, and Oxidative Potential: A Link between Sulfate and Aerosol Toxicity. Environ. Sci. Technol., 51,2611-2620, https://doi.org/10.1021/acs.est.6b06151, 2017.

Fang X, Liu Y, Kejian, Tao W, Yue D, Yiqing F, et al.: Atmospheric Nitrate Formation through Oxidation by carbonate radical. ACS Earth Space Chem., 5,1801–1811, https://doi.org/10.1021/acsearthspacechem.1c00169, 2021.

Feng T, Bei NF, Zhao SY, Wu JR, Li X, Zhang T, et al.: Wintertime nitrate formation during haze days in the Guanzhong basin, China: A case study. Environ. Pollut., 243,1057-1067, https://doi.org/10.1016/j.envpol.2018.09.069, 2018.

Ferrer-Sueta G, Vitturi D, Batinic-Haberle I, Fridovich I, Goldstein S, Czapski G, et al.: Reactions of manganese porphyrins with peroxynitrite and carbonate radical anion. J. Biol. Chem., 278,27432-27438, https://doi.org/10.1074/jbc.M213302200, 2003.

Gankanda A, Coddens EM, Zhang YP, Cwiertny DM, Grassian VH: Sulfate formation catalyzed by coal fly ash, mineral dust and iron(III) oxide: variable influence of temperature and light. Environmental Science-Processes & Impacts, 18,1484-1491, https://doi.org/10.1039/c6em00430j, 2016.

Ge WD, Liu JF, Yi K, Xu JY, Zhang YZ, Hu XR, et al.: Influence of atmospheric in-cloud aqueous-phase chemistry on the global simulation of SO_2 in CESM2. Atmos. Chem. Phys., 21,16093-16120, https://doi.org/10.5194/acp-21-16093-2021, 2021.

Ghalei M, Ma J, Schmidhammer U, Vandenborre J, Fattahi M, Mostafavi M: Picosecond pulse radiolysis of highly concentrated carbonate solutions. J. Phys. Chem. B, 120,2434-2439, https://doi.org/10.1021/acs.jpcb.5b12405, 2016.

Goldstein S, Czapski G, Lind J, Merényi G: Carbonate radical ion is the only observable intermediate in the reaction of peroxynitrite with CO_2. Chem. Res. Toxicol., 14,1273-1276, https://doi.org/10.1021/tx0100845, 2001.

Graedel TE, Weschler CJ: Chemistry within Aqueous Atmospheric Aerosols And Raindrops. J. Geophys. Res., 19,505-539, https://doi.org/10.1029/RG019i004p00505, 1981.

Hanisch F, Crowley JN: Ozone decomposition on Saharan dust: an experimental investigation. Atmos. Chem. Phys. Disscuss., 3,119-130, https://doi.org/10.5194/acp-3-119-2003, 2003.

Hayon E, Treinin A, Wilf J: Electronic spectra, photochemistry, and autoxidation mechanism of the sulfite-bisulfite-pyrosulfite systems. SO_2^-, SO_3^-, SO_4^-, and SO_5^- radicals. J. Am. Chem. Soc., 94,47-57, https://doi.org/10.1021/ja00756a009, 1972.
He J, Xu HH, Balasubramanian R, Chan CY, Wang CJ: Comparison of NO_2 and SO_2 Measurements Using Different Passive Samplers in Tropical Environment. Aerosol Air Qual. Res., 14,355-363, https://doi.org/10.4209/aaqr.2013.02.0055, 2014.
Herrmann H, Ervens B, Jacobi HW, Wolke R, Nowacki P, Zellner R: CAPRAM2.3: A chemical aqueous phase radical mechanism for tropospheric chemistry. J. Atmos. Chem., 36,231-284, https://doi.org/10.1023/A:1006318622743, 2000.
Hossain MD, Huang Y, Yu TH, Goddard Iii WA, Luo Z: Reaction mechanism and kinetics for CO_2 reduction on nickel single atom catalysts from quantum mechanics. Nat. Commun., 11,2256, https://doi.org/10.1038/s41467-020-16119-6, 2020.
Huang HL, Chao W, Lin JJM: Kinetics of a Criegee intermediate that would survive high humidity and may oxidize atmospheric SO_2. Proc. Natl. Acad. Sci. USA, 112,10857-10862, https://doi.org/10.1073/pnas.1513149112, 2015.
Huang JP, Mabury SA: Steady-state concentrations of carbonate radicals in field waters. Environ. Toxicol. Chem., 19,2181-2188, https://doi.org/10.1002/etc.5620190906, 2000.
Huang L, An JY, Koo B, Yarwood G, Yan RS, Wang YJ, et al.: Sulfate formation during heavy winter haze events and the potential contribution from heterogeneous SO_2 + NO_2 reactions in the Yangtze River Delta region, China. Atmos. Chem. Phys., 19,14311-14328, https://doi.org/10.5194/acp-19-14311-2019, 2019.
Huang X, Song Y, Zhao C, Li MM, Zhu T, Zhang Q, et al.: Pathways of sulfate enhancement by natural and anthropogenic mineral aerosols in China. J. Geophys. Res., 119,14165-14179, https://doi.org/10.1002/2014jd022301, 2014.
Hung HM, Hoffmann MR: Oxidation of Gas-Phase SO_2 on the Surfaces of Acidic Microdroplets: Implications for Sulfate and Sulfate Radical Anion Formation in the Atmospheric Liquid Phase. Environ. Sci. Technol., 49,13768-13776, https://doi.org/10.1021/acs.est.5b01658, 2015.
Hung HM, Hsu MN, Hoffmann MR: Quantification of SO_2 oxidation on interfacial surfaces of acidic micro-droplets: Implication for ambient sulfate formation. Environ. Sci. Technol., 52,9079-9086, https://doi.org/10.1021/acs.est.8b01391, 2018.
Itahashi S, Yamaji K, Chatani S, Hayami H: Refinement of Modeled Aqueous-Phase Sulfate Production via the Fe- and Mn-Catalyzed Oxidation Pathway. Atmosphere, 9,132, https://doi.org/10.3390/atmos9040132, 2018.
Kerminen VM, Hillamo R, Teinilä K, Pakkanen T, Allegrini I, Sparapani R: Ion balances of size-resolved tropospheric aerosol samples: implications for the acidity and atmospheric processing of aerosols. Atmos. Environ., 35,5255-5265, https://doi.org/10.1016/S1352-2310(01)00345-4, 2001.
Kim H, Zhang Q, Heo J: Influence of Intense secondary aerosol formation and long range transport on aerosol chemistry and properties in the Seoul Metropolitan Area during spring time Results from KORUS-AQ. Atmos. Chem. Phys. Disscuss., 18,7149–7168, https://doi.org/10.5194/acp-2017-947, 2017.
Koelemeijer R, Homan CD, Matthijsen J: Comparison of spatial and temporal variations of aerosol optical thickness and particulate matter over Europe. Atmos. Environ., 40,5304-5315, https://doi.org/10.1016/j.atmosenv.2006.04.044, 2006.
Kong LD, Zhao X, Sun ZY, Yang YW, Fu HB, Zhang SC, et al.: The effects of nitrate on the heterogeneous uptake of sulfur dioxide on hematite. Atmos. Chem. Phys., 14,9451-9467, https://doi.org/10.5194/acp-14-9451-2014, 2014.
Lehtipalo K, Rondo L, Kontkanen J, Schobesberger S, Jokinen T, Sarnela N, et al.: The effect of acid-base clustering and ions on the growth of atmospheric nano-particles. Nat. Commun., 7,11594, https://doi.org/10.1038/ncomms11594, 2016.
Li BQ, Ma XY, Li QS, Chen WZ, Deng J, Li GX, et al.: Factor affecting the role of radicals contribution at different wavelengths, degradation pathways and toxicity during UV-LED/chlorine process. Chem. Eng. J., 392,124552, https://doi.org/10.1016/j.cej.2020.124552, 2020.
Li KJ, Kong LD, Zhanzakova A, Tong SY, Shen JD, Wang T, et al.: Heterogeneous conversion of SO_2 on nano alpha-Fe_2O_3: the effects of morphology, light illumination and relative humidity. Environ. Sci. Nano., 6,1838-1851, https://doi.org/10.1039/c9en00097f, 2019.
Li L, Chen ZM, Zhang YH, Zhu T, Li S, Li HJ, et al.: Heterogeneous oxidation of sulfur dioxide by ozone on the surface of sodium chloride and its mixtures with other components. J. Geophys. Res., 112,D18301, https://doi.org/10.1029/2006jd008207, 2007.
Li WJ, Shao LY, Shi ZB, Chen JM, Yang LX, Yuan Q, et al.: Mixing state and hygroscopicity of dust and haze particles before leaving Asian continent. J. Geophys. Res., 119,1044-1059, https://doi.org/10.1002/2013jd021003, 2014.
Li X, Yu J, Jaroniec M: Hierarchical photocatalysts. Chem. Soc. Rev., 45,2603-2636, https://doi.org/10.1039/c5cs00838g, 2016.

Li XR, Wang LL, Ji DS, Wen TX, Pan YP, Sun Y, et al.: Characterization of the size-segregated water-soluble inorganic ions in the Jing-Jin-Ji urban agglomeration: Spatial/temporal variability, size distribution and sources. Atmos. Environ., 77,250-259, https://doi.org/10.1016/j.atmosenv.2013.03.042, 2013.

Liao LF, Lien CF, Shieh DL, Chen MT, Lin JL: FTIR study of adsorption and photoassisted oxygen isotopic exchange of carbon monoxide, carbon dioxide, carbonate, and formate on TiO_2. J. Phys. Chem. B, 106,11240-11245, https://doi.org/10.1021/jp0211988, 2002.

Liu JR, Ning A, Liu L, Wang HX, Kurten T, Zhang XH: A pH dependent sulfate formation mechanism caused by hypochlorous acid in the marine atmosphere. Sci.Total. Envrion., 787,147551, https://doi.org/10.1016/j.scitotenv.2021.147551, 2021.

Liu P, Ye C, Xue C, Zhang C, Sun X: Formation mechanisms of atmospheric nitrate and sulfate during the winter haze pollution periods in Beijing: gas-phase, heterogeneous and aqueous-phase chemistry. Atmos. Chem. Phys., 20,4153–4165, https://doi.org/10.5194/acp-20-4153-2020, 2020a.

Liu TT, Hong YW, Li MR, Xu LL, Chen JS, Bian YH, et al.: Atmospheric oxidation capacity and ozone pollution mechanism in a coastal city of southeastern China: analysis of a typical photochemical episode by an observation-based model. Atmos. Chem. Phys., 22,2173-2190, https://doi.org/10.5194/acp-22-2173-2022, 2022a.

Liu TY, Abbatt JPD: Oxidation of sulfur dioxide by nitrogen dioxide accelerated at the interface of deliquesced aerosol particles. Nat. Chem., 13,1173-+, https://doi.org/10.1038/s41557-021-00777-0, 2021.

Liu TY, Clegg SL, Abbatt JPD: Fast oxidation of sulfur dioxide by hydrogen peroxide in deliquesced aerosol particles. Proc. Natl. Acad. Sci. USA, 117,1354-1359, https://doi.org/10.1073/pnas.1916401117, 2020b.

Liu XC, Tang WJ, Chen HN, Guo JM, Tripathee L, Huang J: Observational Study of Ground-Level Ozone in the Desert Atmosphere. B. Environ. Contam. Tox., 108,219-224, https://doi.org/10.1007/s00128-021-03444-9, 2022b.

Liu Y, Wang T, Fang X, Deng Y, Cheng H, Fu H, et al.: Impact of greenhouse gas CO_2 on the heterogeneous reaction of SO_2 on Alpha-Al_2O_3. Chinese Chem. Lett., 31,2712-2716, https://doi.org/10.1016/j.cclet.2020.04.037, 2020c.

Liu YQ, He XX, Duan XD, Fu YS, Dionysiou DD: Photochemical degradation of oxytetracycline: Influence of pH and role of carbonate radical. Chem. Eng. J., 276,113-121, https://doi.org/10.1016/j.cej.2015.04.048, 2015.

Liu ZR, Xie YZ, Hu B, Wen TX, Xin JY, Li XR, et al.: Size-resolved aerosol water-soluble ions during the summer and winter seasons in Beijing: Formation mechanisms of secondary inorganic aerosols. Chemosphere, 183,119-131, https://doi.org/10.1016/j.chemosphere.2017.05.095, 2017.

Long SL, Zeng JR, Li Y, Bao LM, Cao LL, Liu K, et al.: Characteristics of secondary inorganic aerosol and sulfate species in size-fractionated aerosol particles in Shanghai. J. Environ. Sci. China, 26,1040-1051, https://doi.org/10.1016/S1001-0742(13)60521-5, 2014.

Mahajan AS, Li QY, Inamdar S, Ram K, Badia A, Saiz-Lopez A: Modelling the impacts of iodine chemistry on the northern Indian Ocean marine boundary layer. Atmos. Chem. Phys., 21,8437-8454, https://doi.org/10.5194/acp-21-8437-2021, 2021.

McNaughton CS, Clarke AD, Kapustin V, Shinozuka Y, Howell SG, Anderson BE, et al.: Observations of heterogeneous reactions between Asian pollution and mineral dust over the eastern north Pacific during INTEX-B. Atmos. Chem. Phys., 9,8283-8308, https://doi.org/10.5194/acpd-9-8469-2009, 2009.

Merouani S, Hamdaoui O, Saoudi F, Chiha M, Petrier C: Influence of bicarbonate and carbonate ions on sonochemical degradation of Rhodamine B in aqueous phase. J. Hazard Mater., 175,593-599, https://doi.org/10.1016/j.jhazmat.2009.10.046, 2010.

Miller-Schulze JP, Shafer M, Schauer JJ, Heo J, Solomon PA, Lantz J, et al.: Seasonal contribution of mineral dust and other major components to particulate matter at two remote sites in Central Asia. Atmos. Environ., 119,11-20, https://doi.org/10.1016/j.atmosenv.2015.07.011, 2015.

Mogili PK, Kleiber PD, Young MA, Grassian VH: Heterogeneous uptake of ozone on reactive components of mineral dust aerosol: an environmental aerosol reaction chamber study. J. Phys. Chem. A, 110,13799-807, https://doi.org/10.1021/jp063620g, 2006.

Möller F: On the influence of changes in the CO_2 concentration in air on the radiation balance of the Earth's surface and on the climate. J. Geophys. Res., 68,3877-3886, https://doi.org/10.1029/JZ068i013p03877, 1964.

Najafpour N, Afshin H, Firoozabadi B: Dust concentration over a semi-arid region: Parametric study and establishment of new empirical models. Atmos. Res., 243,104995, https://doi.org/10.1016/j.atmosres.2020.104995, 2020.

Nanayakkara CE, Larish WA, Grassian VH: Titanium dioxide nanoparticle surface reactivity with atmospheric gases, CO_2, SO_2, and NO_2: roles of surface hydroxyl groups and adsorbed water in the formation and stability of adsorbed products. J. Phys. Chem. C, 118,23011-23021, https://doi.org/10.1021/jp504402z, 2014.

Neta P, Huie RE: Free-radical chemistry of sulfite. Environ. Health Persp., 64,209-217, https://doi.org/10.1289/ehp.8564209, 1985.

Nie W, Wang T, Xue LK, Ding AJ, Wang XF, Gao XM, et al.: Asian dust storm observed at a rural mountain site in southern China: chemical evolution and heterogeneous photochemistry. Atmos. Chem. Phys., 12,11985-11995, https://doi.org/10.5194/acp-12-11985-2012, 2012.

None: In-Situ Characterization of Heterogeneous Catalysts. Focus on Catal., 2013,8, https://doi.org/10.1016/S1351-4180(13)70477-X, 2013.

Palmer CD, Cherry JA: Geochemical Evolution of Groundwater in Sequences of Sedimentary-Rocks. J. Hydrol., 75,27-65, https://doi.org/10.1016/0022-1694(84)90045-3, 1984.

Peters SJ, Ewing GE: Water on Salt: An Infrared Study of Adsorbed H_2O on NaCl (100) under Ambient Conditions. J. Phys. Chem. B, 101,10880-10886, https://doi.org/10.1021/jp972810b, 1997.

Rodriguez JA, Hanson J, Chupas P: In-Situ Characterization of Heterogeneous Catalysts. Focus on Catal., 2013,8, https://doi.org/10.1002/9781118355923, 2013.

Rubasinghege G, Elzey S, Baltrusaitis J, Jayaweera PM, Grassian VH: Reactions on Atmospheric Dust Particles: Surface Photochemistry and Size-Dependent Nanoscale Redox Chemistry. J. Phys. Chem. Lett., 1,1729-1737, https://doi.org/10.1021/jz100371d, 2010.

Salama SB, Natarajan C, Nogami G, Kennedy JH: The role of reducing agent in oxidation reactions of water on illuminated TiO_2 electrodes. J. Electrochem. Soc., 142,806-810, https://doi.org/10.1149/1.2048539, 1995.

Samuni A, Goldstein S, Russo A, Mitchell JB, Krishna MC, Neta P: Kinetics and mechanism of hydroxyl radical and OH-adduct radical reactions with nitroxides and with their hydroxylamines. J. Am. Chem. Soc., 124,8719-8724, https://doi.org/10.1021/ja017587h, 2002.

Shafirovich V, Dourandin A, Huang W, Geacintov NE: The carbonate radical is a site-selective oxidizing agent of guanine in double-stranded oligonucleotides. J. Biol. Chem., 276,24621-24626, https://doi.org/10.1074/jbc.M101131200, 2001.

Shang J, Li J, Zhu T: Heterogeneous reaction of SO_2 on TiO_2 particles. Sci. China Chem., 53,2637-2643, https://doi.org/10.1007/s11426-010-4160-3, 2010.

Song X, Li J, Shao L, Zheng Q, Zhang D: Inorganic ion chemistry of local particulate matter in a populated city of North China at light, medium, and severe pollution levels. Sci.Total. Envrion., 650,566-574, https://doi.org/10.1016/j.scitotenv.2018.09.033, 2018.

Stenman D, Carlsson M, Jonsson M, Reitberger T: Reactivity of the carbonate radical anion towards carbohydrate and lignin model compounds. J. Wood Chem. Technol., 23,47-69, https://doi.org/10.1081/Wct-120018615, 2003.

Stevenson DS, Zhao A, Naik V, O'Connor FM, Tilmes S, Zeng G, et al.: Trends in global tropospheric hydroxyl radical and methane lifetime since 1850 from AerChemMIP. Atmos. Chem. Phys., 20,12905-12920, https://doi.org/10.5194/acp-20-12905-2020, 2020.

Stone R: Air pollution. Counting the cost of London's killer smog. Science, 298,2106-2107, https://doi.org/10.2307/3833025, 2002.

Su H, Cheng Y, Zheng G, Wei C, Mu Q, Zheng B, et al.: Reactive nitrogen chemistry in aerosol water as a source of sulfate during haze events in China. Sci. Adv., 2,e1601530, https://doi.org/10.1126/sciadv.1601530, 2016.

Su WG, Zhang J, Feng ZC, Chen T, Ying PL, Li C: Surface phases of TiO_2 nanoparticles studied by UV Raman spectroscopy and FT-IR spectroscopy. J. Phys. Chem. C, 112,7710-7716, https://doi.org/10.1021/jp7118422, 2008.

Sullivan RC, Guazzotti SA, Sodeman DA, Prather KA: Direct observations of the atmospheric processing of Asian mineral dust. Atmos. Chem. Phys., 7,1213-1236, https://doi.org/10.5194/acp-7-1213-2007, 2007.

Sulzberger B, Canonica S, Egli T, Giger W, Klausen J, Gunten Uv: Oxidative transformations of contaminants in natural and in technical systems. Chimia, 51,900-907, https://doi.org/10.1051/epjconf/20101105003, 1997.

Sun P, Tyree C, Huang CH: Inactivation of Escherichia coli, Bacteriophage MS2, and Bacillus Spores under UV/H_2O_2 and UV/Peroxydisulfate Advanced Disinfection Conditions. Environ. Sci. Technol., 50,4448-4458, https://doi.org/10.1021/acs.est.5b06097, 2016.

Ta WQ, Xiao Z, Qu JJ, Yang GS, Wang T: Characteristics of dust particles from the desert/Gobi area of northwestern China during dust-storm periods. Environmental Geology, 43,667-679, https://doi.org/10.1007/s00254-002-0673-1, 2003.

Tang MJ, Cziczo DJ, Grassian VH: Interactions of Water with Mineral Dust Aerosol: Water Adsorption, Hygroscopicity, Cloud Condensation, and Ice Nucleation. Chem. Rev., 116,4205-4259, https://doi.org/10.1021/acs.chemrev.5b00529, 2016.

Wang XM, Huang X, Zuo CY, Hu HY: Kinetics of quinoline degradation by O_3/UV in aqueous phase. Chemosphere, 55,733-741, https://doi.org/10.1016/j.chemosphere.2003.11.019, 2004.

Wang Y, Wan Q, Meng W, Liao F: Long-term impacts of aerosols on precipitation and lightning over the Pearl River Delta megacity area in China. Atmos. Chem. Phys., 11,12421-12436, https://doi.org/10.5194/acp-11-12421-2011, 2011.

Wang Y, Zhuang GS, Tang AH, Yuan H, Sun YL, Chen SA, et al.: The ion chemistry and the source of PM2.5 aerosol in Beijing. Atmos. Environ., 39,3771-3784, https://doi.org/10.1016/j.atmosenv.2005.03.013, 2005.

Wang YX, Zhang QQ, Jiang JK, Zhou W, Wang BY, He KB, et al.: Enhanced sulfate formation during China's severe winter haze episode in January 2013 missing from current models. J. Geophys. Res., 119,10425-10440, https://doi.org/10.1002/2013jd021426, 2014.

Watanabe K, Yang L, Nakamura S, Otani T, Mori K: Volcanic Impact of Nishinoshima Eruptions in Summer 2020 on the Atmosphere over Central Japan: Results from Airborne Measurements of Aerosol and Trace Gases. Sola, 17,109-112, https://doi.org/10.2151/sola.2021-017, 2020.

Wei J, Yu H, Wang Y, Verma V: Complexation of Iron and Copper in Ambient Particulate Matter and Its Effect on the Oxidative Potential Measured in a Surrogate Lung Fluid. Environ. Sci. Technol., 53,1661-1671, https://doi.org/10.1021/acs.est.8b05731, 2019.

Witkowska A, Lewandowska AU, Saniewska D, Falkowska LM: Effect of agriculture and vegetation on carbonaceous aerosol concentrations ($PM_{2.5}$ and PM_{10}) in Puszcza Borecka National Nature Reserve (Poland). Air Qual Atmos Hlth, 9,761-773, https://doi.org/10.1007/s11869-015-0378-8, 2016.

Wojnarovits L, Toth T, Takacs E: Rate constants of carbonate radical anion reactions with molecules of environmental interest in aqueous solution: A review. Sci.Total. Envrion., 717,137219, https://doi.org/10.1016/j.scitotenv.2020.137219, 2020.

Wu C, Zhang S, Wang G, Lv S, Li D, Liu L, et al.: Efficient Heterogeneous Formation of Ammonium Nitrate on the Saline Mineral Particle Surface in the Atmosphere of East Asia during Dust Storm Periods. Environ. Sci. Technol., 54,15622-15630, https://doi.org/10.1021/acs.est.0c04544, 2020.

Wu D, Fan Z, Ge X, Meng Y, Xia J, Liu G, et al.: Chemical and Light Extinction Characteristics of Atmospheric Aerosols in Suburban Nanjing, China. Atmosphere, 8,149, https://doi.org/10.3390/atmos8080149, 2017.

Wu LY, Tong SR, Wang WG, Ge MF: Effects of temperature on the heterogeneous oxidation of sulfur dioxide by ozone on calcium carbonate. Atmos. Chem. Phys., 11,6593-6605, https://doi.org/10.5194/acp-11-6593-2011, 2011.

Wu Q, Tang X, Kong L, Dao X, Lu MM, Liu ZR, et al.: Evaluation and Bias Correction of the Secondary Inorganic Aerosol Modeling over North China Plain in Autumn and Winter. Atmosphere, 12,578, https://doi.org/10.3390/atmos12050578, 2021.

Xia DM, Zhang XR, Chen JW, Tong SR, Xie HB, Wang ZY, et al.: Heterogeneous Formation of HONO Catalyzed by CO_2. Environ. Sci. Technol., 55,12215-12222, https://doi.org/10.1021/acs.est.1c02706, 2021.

Xiong XQ, Zhang X, Xu YM: Incorporative Effect of Pt and Na_2CO_3 on TiO_2-Photocatalyzed Degradation of Phenol in Water. J. Phys. Chem. C, 120,25689-25696, https://doi.org/10.1021/acs.jpcc.6b07951, 2016.

Yan JF, Peng JL, Lai LD, Ji FZ, Zhang YH, Lai B, et al.: Activation $CuFe_2O_4$ by Hydroxylamine for Oxidation of Antibiotic Sulfamethoxazole. Environ. Sci. Technol., 52,14302-14310, https://doi.org/10.1021/acs.est.8b03340, 2018.

Yan SW, Liu YJ, Lian LS, Li R, Ma JZ, Zhou HX, et al.: Photochemical formation of carbonate radical and its reaction with dissolved organic matters. Water Res., 161,288-296, https://doi.org/10.1016/j.watres.2019.06.002, 2019.

Yermakov AN, Purmal AP: Iron-catalyzed oxidation of sulfite: From established results to a new understanding. Prog. React. Kinet. Mec., 28,189-255, https://doi.org/10.3184/007967403103165503, 2003.

Yu T, Zhao D, Song X, Zhu T: NO_2-initiated multiphase oxidation of SO_2 by O_2 on $CaCO_3$ particles. Atmos. Chem. Phys., 18,6679-6689, https://doi.org/10.5194/acp-18-6679-2018, 2018.

Yu ZC, Jang MS, Kim S, Bae C, Koo BY, Beardsley R, et al.: Simulating the Impact of Long-Range-Transported Asian Mineral Dust on the Formation of Sulfate and Nitrate during the KORUS-AQ Campaign. ACS Earth Space Chem., 4,1039-1049, https://doi.org/10.1021/acsearthspacechem.0c00074, 2020.

Zhang GS, He XX, Nadagouda MN, O'Shea KE, Dionysiou DD: The effect of basic pH and carbonate ion on the mechanism of photocatalytic destruction of cylindrospermopsin. Water Res., 73,353-361, https://doi.org/10.1016/j.watres.2015.01.011, 2015a.

Zhang R, Wang G, Song G, Zamora ML, Qi Y, Yun L, et al.: Formation of urban fine particulate matter. Chem. Rev., 115,3803-3855, https://doi.org/10.1021/acs.chemrev.5b00067, 2015b.

Zhang T, Cao JJ, Tie XX, Shen ZX, Liu SX, Ding H, et al.: Water-soluble ions in atmospheric aerosols measured in Xi'an, China: Seasonal variations and sources. Atmos. Res., 102,110-119, https://doi.org/10.1016/j.atmosres.2011.06.014, 2011.

Zhang Y, Carmichael GR: The role of mineral aerosol in tropospheric chemistry in East Asia - A model study. J. Appl. Meteorol. Clim., 38,353-366, https://doi.org/10.1175/1520-0450(1999)038<0353:Tromai>2.0.Co;2, 1999.

Zheng B, Zhang Q, Zhang Y, He KB, Wang K, Zheng GJ, et al.: Heterogeneous chemistry: a mechanism missing in current models to explain secondary inorganic aerosol formation during the January 2013 haze episode in north China. Atmos. Chem. Phys., 15,2031-2049, https://doi.org/10.5194/acp-15-2031-2015, 2015.